Primary U-distribution in scleractinian corals and its implications for U-series dating

Laura F. Robinson[1], Jess F. Adkins[1], Diego P. Fernandez[1], Donald S. Burnett[1], S-L Wang[1], Alexander C. Gagnon[1] and Nir krakauer[1]

1: California Institute of Technology, MS 100-23, 1200 E. California Boulevard, Pasadena, CA 91125

Index terms: 1120, 1040, 4916

Key words: uranium, diagenesis, dating, coral

Main text words: 5,488

ABSTRACT

In this study we use micro-sampling techniques to explore diagenetic processes in carbonates which are important as they can affect the accuracy to U-series chronometry. Fission track maps of deep-sea scleractinian corals show a 3-fold difference between the minimum and maximum [U] in modern corals, which is reduced to a factor of 2 in fossil corals. We use micro-milling and MC-ICP-MS to make detailed analyses of the [U] and $\delta^{234}U_{initial}$ distributions in corals from 218 ka to modern. Within each fossil coral we observe a large range of $\delta^{234}U_{initial}$ values, with high $\delta^{234}U_{initial}$ associated with low [U]. A simple model shows that this observation is best explained by preferential movement of alpha-decay produced ^{234}U ($^{234}U^{AR}$) atoms. Addition of ^{234}U with no ^{238}U may occur by coupling a high [U] surface layer, probably organic, with preferential movement of $^{234}U^{AR}$. This process leads to large, whole-coral $\delta^{234}U_{initial}$ elevations with little effect on the final age. The diagenetic processes that we model are relevant both to surface and deep-sea scleractinian corals since both exhibit primary [U] heterogeneity and may be subject to U-addition.

INTRODUCTION

U-series isotopes in biogenic carbonates provide vital information in our understanding of past climate. Probably the most important application is the use of U decay to Th and Pa which provides two precise chronometers suited to dating climate events over the last few hundred thousand years *[Broecker*, 1963; *Edwards et al.*, 1986; *Stirling et al.*, 1995; *Edwards et al.*, 1997]. In addition to dating, the uranium concentration in carbonates has been used to constrain past water mass properties *[Min et al.*, 1995; *Shen & Dunbar*, 1995; *Russell et al.*, 2004] and uranium isotope variability has also been linked to past climate and weathering patterns *[Robinson et al.*, 2004b]. To make full use of U-series isotopes in ancient carbonates we must understand the two key controls on the final, measured U-series distribution; the initial incorporation and any subsequent diagenesis.

Uranium is found as a trace metal in both calcite and aragonite *[Djogic et al.*, 1987; *Pingitore et al.*, 2002]. The octahedral shape of the tetravalent uranyl carbonate ion is, however, more readily included in the aragonite lattice than the calcite lattice *[Reeder et al.*, 2001]. The resulting high uranium content of aragonite makes the skeletons of scleractinian corals ideally suited to precise U-series measurements. Surface corals have a heterogeneous U distribution that typically follows the growth banding and displays a negative correlation to growth temperature *[Min et al.*, 1995]. This relationship can be complicated by a number of other parameters such as pH at the calcification site, carbonate ion concentration, or growth rate *[Shen & Dunbar*, 1995]. Modern surface corals display two additional types of uranium heterogeneity that have not been linked to environmental controls: enrichment by up to a factor of two at septal edges and "random" small scale variations *[Schroeder et al.*, 1970].

An obvious test of whether diagenesis affects the primary U-distribution is to compare modern and fossil samples of similar material. Modern corals have typical [U] (U-concentration) of 2-3.5 ppm *[Shen & Dunbar*, 1995]. Within 1 kyr of death, the coral pores can become partially filled with

aragonite that is enriched in uranium relative to the original coral skeleton *[Lazar et al.*, 2004]. Swart & Hubbard (1982) showed that fossil corals had [U] up to 6 ppm in areas that had been affected by endolithic sponge borings *[Swart & Hubbard*, 1982]. They also showed that dead, non-bioeroded corals soaked in concentrated U solutions developed U-enrichment along skeletal margins and trabecular centres demonstrating a rapid diagenetic pathway for U-addition.

A second measure of diagenetic activity is the U isotope activity ratio ($^{234}U/^{238}U$). Marine carbonates incorporate the isotopic ratio (denoted as $\delta^{234}U$ (=([($^{234}U/^{238}U)_{meas}/(^{234}U/^{238}U_{eq})$]-1)x$10^3$) of the seawater in which they grow (e.g. *[Broecker & Takahashi*, 1966; *Robinson et al.*, 2004a]). This value is constant throughout the water column [*Cheng et al.*, 2000a] and has been constant (~146 ‰) to within ~ 10 ‰ over the last several hundred thousand years *[Bard et al.*, 1991; *Stirling et al.*, 1995; *Henderson*, 2002]. For a closed system, the $\delta^{234}U_{initial}$ ($\delta^{234}U_{initial} = \delta^{234}Ue^{\lambda t}$) should be identical to that of the modern day *[Edwards et al.*, 1986]. However, the $\delta^{234}U_{initial}$ values of carbonates exhibit increasing scatter, and tend to be more elevated, at greater ages (Figure 1 e.g. *[Bender et al.*, 1979; *Henderson*, 2002]. These differences have been attributed to diagenesis, and the associated U-Th ages are, therefore, potentially unreliable *[Gallup et al.*, 1994]. However, this indicator does not necessarily guarantee a reliable age, since paired U-Th and U-Pa ages with a "good" $\delta^{234}U_{initial}$ can return different ages. Conversely, some concordant U-Th, U-Pa ages have "bad" $\delta^{234}U_{initial}$ values *[Cutler et al.*, 2003]. This observation means that we must look carefully at the processes of U-series re-distribution, gain and loss if we are to generate accurate ages.

A number of models have been developed to try and back calculate meaningful ages from diagenetically altered carbonates *[Bender et al.*, 1979; *Gallup et al.*, 1994; *Henderson et al.*, 2001; *Thompson et al.*, 2003; *Villemant & Feuillet*, 2003; *Scholz et al.*, 2004]. Bender et al (1979) and Gallup et al (1994) explain the isotopic trends observed in Barbados corals through addition of ^{234}U

and ^{230}Th. Scholz et al. (2004) model a suite of corals that have been exposed to meteoric waters through some of their post-mortem history. They apply episodic pulses of U loss and gain, with the δ^{234}U of the added uranium determined by making multiple measurements on sub-samples from the same coral. This empirical model reveals the diagenetic history of a single coral, but is clearly not able to explain the $\delta^{234}U_{initial}$ distribution of corals from a wide range of environments.

Henderson et al. (2001) observed variable δ^{234}U in mineral separates from carbonate sediments and developed a model allowing preferential movement of isotopes produced by alpha recoil (^{234}Th and ^{230}Th) between sedimentary grains with different [U]. Both Thompson et al. (2003) and Villemant & Feuillet (2003) developed models based on this process of alpha-recoil mobilisation. Villemant & Feuillet propose a model with continuous gain or loss of ^{234}U, ^{234}Th and ^{230}Th and allow for the possibility of initial ^{230}Th in the coral skeleton. Thompson et al. (2003) model the transport of decay produced ^{230}Th or ^{234}Th from one sample to another. Th produced by decay in one coral may be implanted directly onto another coral, alternatively this Th, or Th produced in the pore water itself, may be transported by the pore waters and then adsorbed onto a secondary coral sample. The model assumes that the samples gaining and losing uranium have identical ages and $\delta^{234}U_{initial}$ values, for example in an ancient reef setting. Thompson et al (2003) use their model to generate broadly consistent open-system ages for data from corals from uplifted terraces in a number of locations.

The Thompson et al. (2003) model works well for calculating ages for numerous corals from the same terrace that are assumed to have formed at the same time *[Thompson & Goldstein*, 2005]. However, it is less good at explaining the range of $\delta^{234}U_{initial}$ values measured in replicate sub-samples of single corals. For example, application of this open-system model to replicate data in Cutler et al (2003) causes the age variance between sub-samples to increase in 11 out of 15 cases compared to traditional closed-system ages. The problem lies in the fact that some sub-samples

with $\delta^{234}U_{initial}$ variability of 6 ‰ have the same U-Th age, but the model predicts a tight correlation between closed-system age and $\delta^{234}U_{initial}$. Clearly there is more than one diagenetic process that can affect these fossil carbonates. The model setting, an ancient reef, allows any coral to act either as a net source or net sink of Th, the extent of loss or gain being estimated from the $\delta^{234}U_{initial}$. However, the observation that most corals are enriched in ^{234}U raises the question of completing the mass balance requirements for U and Th across the reef setting. Finally, two of the transfer mechanisms rely on transport of Th, which is known to be less mobile than uranium in oxic aqueous settings.

Deep-sea scleractinian corals may provide us with a key to understanding both primary U incorporation and the mechanisms controlling its redistribution with time. Comparison of the isotopic content of surface and deep-sea corals suggests that they are affected by similar diagenetic processes (Figure 1). In this study we use solitary, ahermatypic, cone-shaped scleractinian corals of the species *Desmophyllum dianthus* (formerly known as *Desmophyllum cristagalli*) to investigate U-series diagenesis. Each individual is thought to have a lifetime of some 100 years *[Adkins et al.*, 2004] and so we do not expect to see large or cyclic changes in the ambient growth temperature or chemical composition of the surrounding seawater except at times of rapid climate change. Primary [U] variability is therefore expected to be controlled by physiological processes, so called "vital effects". Throughout their diagenetic history the corals are bathed in seawater with unchanging [U] and $\delta^{234}U$, so open-system behaviour must be the result of bioerosion or interaction with seawater.

In addition to informing us about diagenesis in surface scleractinian corals, we are interested in understanding deep-sea coral chemistry as these corals form unique, directly-datable records of the deep ocean ([*Adkins et al.*, 1998; *Lomitschka & Mangini*, 1999; *Cheng et al.*, 2000a; *Goldstein et al.*, 2001; *Frank et al.*, 2004] *[Smith et al.*, 2000]). In this study we use two approaches to test the

assumptions made in dating biogenic carbonates; we compare whole coral U-Th isotope measurements from surface and deep-sea corals and we map out the [U] and $\delta^{234}U$ distribution on the 10s μm scale in modern and fossil deep-sea corals over a 218 kyr time period.

METHODS

Multiple polished thin sections from two corals (modern and 33 ka) were mounted flush against micas and subjected to neutron bombardment to induce fission of ^{235}U *[Murrell & Burnett*, 1982]. The coral sections experienced fluences of either $1x10^{16}$ cm^{-2} or $5x10^{16}$ cm^{-2}. The resulting fission tracks recorded on the mica were etched in concentrated HF for 25-30 minutes, and imaged by scanning electron microscopy (SEM). The relative [U] is determined by dividing the coral into equal area boxes and counting the number of fission tracks using NIH-ImageJ software. The size of these boxes, 25x200μm was chosen to give a minimum of 100 counts in low [U] areas with associated counting statistics of 10% and an associated sample resolution of ~25 μm perpendicular to the banding. The isentropic production of fission products from a single ^{235}U atom can limit our spatial resolution by producing tracks on the mica in a wider area than the position of the point source. Based on an estimate of the path length of the fission products in the aragonite we estimate our minimum spatial resolution to be about 10 μm.

Thin sections of one modern and six fossil corals of known age (10.9 ka, 14.8 ka, 16.2 ka, 43.9 ka, 83.0 ka and 218.5 ka) were polished and sampled by micro-milling to give sample masses of ~1 mg, and a typical spatial resolution of 100-400 μm perpendicular to the banding (Figure 2). Each sample was weighed, spiked using a pure ^{236}U spike, dissolved and taken through anion-exchange chemistry *[Edwards et al.*, 1986]. The purified uranium was re-dissolved in 5% nitric acid and aspirated into a Neptune multi-collector inductively coupled mass spectrometer (MC-ICP-MS) (Robinson et al submitted). There is insufficient ^{230}Th to allow age measurements of each

individual sub-sample, so the age of the whole coral is used to calculate $\delta^{234}U_{initial}$. Eighty-five whole coral samples of ~1 g were cleaned to remove the ferromanganese coating following the procedure of Cheng et al (2000), spiked using a ^{236}U-^{229}Th mixed spike and analysed for U and Th using MC-ICP-MS *[Robinson et al.*, submitted].

RESULTS

D dianthus has a complex banding pattern which is controlled by the calcification of the coral and is apparent both visually [*Lazier et al.*, 1999] and in some aspects of its chemical composition [*Adkins et al.*, 2003]. The aragonite in the central growth band of each septum comprises irregular fine-grained crystals which are surrounded by bunches of acicular crystals as seen in the etched and untreated SEM images in Figures 3a and b. In the central band of the etched SEM image there are two dark coloured features whose amorphous shape suggests an organic origin (Figure 2a). These features (called spheres) are observed at the centre of the granular aragonite, and when stacked-up in a thin section are probably the cause of the dark banding seen in transmitted light images (Figures 3c and d).

The [U] distribution in modern *D. dianthus* is heterogeneous, and has a spatial structure coherent with the visible banding. This coherency is best seen by comparing a fission track map and a transmitted light image of the same coral section (Figure 4). The central part of the coral septum is depleted in uranium, but the zone of depletion is wider than the transmitted light banding over and above the 10 μm spatial resolution (Figure 4). The fission track density variations show that the modern coral difference between minimum and maximum [U] is greater than a factor of 3 (Figure 5, Figure 6). Fission track maps from a 33 ka fossil coral display a similar U distribution to the modern coral, but the contrast between U-depleted and U-enriched aragonite is significantly reduced, to at most a factor of 2 (Figure 6). The fission track maps shown in Figures 4, 5 and 6 are

typical of the [U] distribution measured multiple times in each coral, ruling out analytical artefacts such as a bad contact between the coral and mica as the cause of the contrast between modern and fossil corals.

Micro-milling integrates across a wider spatial scale (100-400 μm) than the fission tracks and so may not capture the full [U] range. However, the [U] patterns are consistent with fission track data and have a typical range of 2.5 – 5.5 ppm (Table 1). Endolithic sponge borings in the 11 ka coral have a brown discolouration and a measured [U] of 15 ppm (Figure 2). No bioeroded samples were analysed using fission tracks, so we do not know the micro-scale spatial distribution of uranium within such bioeroded areas. Whole coral [U] range from 2.3-7.0 ppm with an average of 3.9 ppm and there is no correlation between the age of the sample and the [U] (Figure 7).

Micro-milled corals were analysed for $\delta^{234}U$ as well as [U]. The integrated $\delta^{234}U$ of the modern, micro-milled coral averages 145±2.2, identical to the seawater value (Figure 8). By contrast, individual micro-milled coral samples have a wide range of $\delta^{234}U_{initial}$ values, from 137-221‰ (Table 2). Whole fossil coral analyses have a similar $\delta^{234}U_{initial}$ range, 138-210 ‰. In both whole coral and micro-milled measurements, high $\delta^{234}U_{initial}$ values tend to be associated with low [U] (Figure 8). The same data are plotted with distance along the coral perpendicular to the banding to show the spatial distribution of [U] and $\delta^{234}U_{initial}$ for five of the micro-milled fossil corals (Figure 9). The highest $\delta^{234}U_{initial}$ is observed in the central band for three out of four septal samples. Two corals (43 ka and 83 ka) have no whole coral $\delta^{234}U_{initial}$ elevation, but show internal $\delta^{234}U_{initial}$ ranges of 140-155 ‰ and 137-163 ‰ respectively. The 11 ka, 16 ka and 218 ka sections have whole coral $\delta^{234}U_{initial}$ values and ranges of 150 ‰ (146-160 ‰), 152 ‰ (148-159 ‰) and 161 ‰ (150-221 ‰) respectively.

DISCUSSION

We model a range of diagenetic process in a simple box model, and then apply the results to measured coral sections. In the first part of the discussion we use the evidence of coherent, primary [U] heterogeneity coupled with development of $\delta^{234}U_{initial}$ gradients over time to model internal processes that affect the distribution of U and Th in the carbonate structure. These processes are radioactive decay, diffusion and direct transfer of alpha-recoil decay products. In the second part of the discussion we investigate open-system behaviour. This second class of processes add uranium to the coral, and so have the potential to alter the apparent whole coral age.

The model is set up as a series of parallel 50 μm boxes with each isotope ^{238}U, ^{230}Th, $^{234}U^{i}$ (^{234}U present in the primary coral structure) and $^{234}U^{AR}$ (^{234}U produced by decay) considered separately. In the sensitivity studies we use 25 boxes with their initial U-distribution based on fission tracks and micro-milling, all with $\delta^{234}U_{initial}$ of 146 and ^{230}Th of zero (Figure 10). We run the model for 20 kyr and 200 kyr to investigate the cumulative effects of each of these processes over time. The model results are plotted as $\delta^{234}U_{initial}$ versus [U] so that the central boxes in Figure 11 plot at low [U] and the outer boxes plot at high [U], allowing direct comparison with the measured data shown in Figure 8. We apply the model results to five real coral sections to assess the implication of closed and open system diagenesis on $\delta^{234}U_{initial}$ and age.

Closed system U and Th processes

In a closed system we are considering the internal reorganisation of U and Th isotopes. With no net loss or gain of U or Th the age and $\delta^{234}U_{initial}$ of the whole coral will not be affected. The most obvious internal process is radioactive decay, governed by the activity of the isotopes. The energy produced by alpha decay gives recoil momentum to the alpha particle and also to the daughter isotope which has an expected recoil length scale (L_R) on the order 0.1μm *[Kigoshi*, 1971]. The

amount of ^{234}Th and ^{230}Th that is moved by recoil-momentum is controlled by the activity of the respective parent isotopes ^{238}U and ^{234}U, and the recoil length scale. The net transfer is from areas of high to low parent concentration, leading to isotopic variability across the coral. In contrast to previous models, we are able to calculate the exact extent of this process as we know both the length scale of recoil (L_R) and the length scale of the primary [U] heterogeneity. We allow half of the decays within the recoil length scale to escape to the neighbouring box to account for the random directionality of the recoil-momentum. The equation below describes the direct alpha-recoil flux in and out ($F^{in}_{\alpha\_r}$ and $F^{out}_{\alpha\_r}$) of a box 'j' of length L_B.

$$\frac{dN^{j}}{dt} = F^{in}_{\alpha\_r} - F^{out}_{\alpha\_r} = 0.5\lambda_{parent}\frac{L_R}{L_B}\left[-2.N^{j}_{parent} + N^{j-1}_{parent} + N^{j+1}_{parent}\right] \qquad \text{(Equation 1)}$$

Since the net transfer of ^{230}Th and ^{234}Th is dependent on the ^{238}U and ^{234}U concentration gradient, this process will lead to elevated $\delta^{234}U_{initial}$ in low [U] zones as observed in the coral sections. However, the 500-fold disparity between recoil length scale and sampling length scale means that direct transfer only produces sub-per mil $\delta^{234}U_{initial}$ deviations at 200 ka (Figure 11a). This is not a strictly closed system process because daughter isotopes can be expelled from the edges of the coral but the small number of atoms expelled has a negligible effect on the whole coral $\delta^{234}U_{initial}$ or age.

The presence of [U] gradients may cause diffusive movement of uranium which would produce smooth profiles unlike the observed fossil fission track pattern. The diffusion coefficients for solid state diffusion of Sr and Pb in calcite at 300 K are ~ $2x10^{-24}$ $\mu m^2 yr^{-1}$ and $2\ x10^{-23}$ $\mu m^2 yr^{-1}$ respectively, and U is likely to be of a similar magnitude *[Cherniak*, 1997]. Additionally, if U has to diffuse as a hexavalent carbonate complex, it might be even slower. Solid-state diffusion of U through the crystal lattice is therefore, expected to be negligible on these 10^4-10^5 year timescales.

In any case, if ^{234}U and ^{238}U diffuse at the same rate, then diffusion cannot lead to isotopic gradients. However, if ^{238}U and part of the ^{234}U ($^{234}U^{AR}$) have different apparent diffusion coefficients then we would expect to see isotopic gradients develop over time. The recoil energy given to the ^{234}Th daughter from a ^{238}U decay is sufficient to displace it from lattice sites, in many cases to an interstitial location. Thus, the $^{234}U^{AR}$ that has been produced through decay from ^{234}Th is more mobile than its parent ^{238}U *[Fleischer*, 1988], leading to a situation where $^{234}U^{AR}$ has a faster diffusion coefficient than ^{238}U. We model this process by allowing $^{234}U^{AR}$ atoms to move through the coral, but not allowing the $^{234}U^{i}$ and ^{238}U atoms that were incorporated in the original aragonite to diffuse.

The mineral texture of the coral is likely to influence the rate of $^{234}U^{AR}$ mobility so we use two different diffusion coefficients, D^{AR}; 0.5 $\mu m^2 yr^{-1}$ in the fine, granular aragonite and the slower rate of 0.1 $\mu m^2 yr^{-1}$ in the larger grained acicular material. In our sensitivity study these are the diffusion coefficients required to produce $\delta^{234}U_{initial}$ values of up to 151 ‰ (20 ka) and 458 ‰ (200 ka) in the low [U] zones (Figure 11b). During the course of the model run $^{234}U^{Ar}$ atoms move down the concentration gradient causing build up of $^{234}U^{AR}$ in the low [U] central band. This movement results in the lowest $\delta^{234}U_{initial}$ values being in the boxes immediately adjacent to the central band. The diffusion coefficients for diffusion in water and in sedimentary pore fluids are on the order of 1000 $\mu m^2 yr^{-1}$ and 100 $\mu m^2 yr^{-1}$ respectively, several orders of magnitude higher than the values we use for D^{AR} [*Li & Gregory*, 1974]. However D^{AR} is much closer in magnitude to diffusion in pore fluids than to solid state diffusion suggesting that water may play a role in the movement of $^{234}U^{AR}$ through the coral. Grain boundary diffusion is also a possible movement mechanism, but our data set does not allow us to distinguish between these separate pathways. We take the simple approach of assigning one diffusion coefficient to each mineral type for all of our model runs.

These model results demonstrate that the presence of [U] gradients within a coral structure can lead to large isotopic gradients, not just $\delta^{234}U_{initial}$ but also ($^{230}Th/^{238}U$) ratios. If the whole coral sample is analysed, an accurate age with a $\delta^{234}U_{initial}$ of 146.5 will be measured. However, if the sampling is biased towards one part of the coral, the resulting age is likely to be inaccurate. For example in the 200 kyr sensitivity study with preferential movement of $^{234}U^{AR}$ the ages of individual boxes range from 157 ka to 213 ka. In this case, age biases of thousands of years are not unreasonable.

Two measured fossil coral sections, 43 ka and 83 ka do not exhibit whole coral $\delta^{234}U_{initial}$ elevation, and so the $\delta^{234}U_{initial}$ variability in the micro-milled samples is likely to be a result of internal reorganisation of U and Th only. Therefore we model both corals allowing decay, direct transfer of alpha-decay products and preferential movement of $^{234}U^{AR}$ with D^{AR} values of 0.5 $\mu m^2 yr^{-1}$ and 0.1 $\mu m^2 yr^{-1}$ in the granular and acicular aragonite respectively. The equation for each isotope follows the form:

$$\frac{dN_{238}}{dt} = -\lambda_{238} N_{238} \qquad \text{(Equation 2)}$$

$$\frac{dN^{i}_{234}}{dt} = -\lambda_{234} N^{i}_{234} \qquad \text{(Equation 3)}$$

$$\frac{dN^{AR}_{234}}{dt} = \lambda_{238} N_{238} - \lambda_{234} N^{AR}_{234} + \left(\frac{d}{dz} D^{AR} \frac{dN^{AR}_{234}}{dz} \right) + F^{in}_{\alpha\_r} - F^{out}_{\alpha\_r} \qquad \text{(Equation 4)}$$

$$\frac{dN_{230}}{dt} = \lambda_{234} N^{i}_{234} + \lambda_{234} N^{AR}_{234} - \lambda_{230} N_{230} + F^{in}_{\alpha\_r} - F^{out}_{\alpha\_r} \qquad \text{(Equation 5)}$$

The 43 ka coral model results are remarkably similar to the observations, both spatially and in total $\delta^{234}U_{initial}$ range (Figure 12a). During sampling of the 83 ka coral we did not achieve 100% recovery on some of the powder samples, leading to inaccurate [U] (Table 2), so the initial boundary conditions are not as well constrained in this sample. However, assuming a reasonable [U]

distribution and applying the model again returns a spatial pattern and $\delta^{234}U_{initial}$ range that is, again, very similar to the observations (Figure 12b).

Open system behaviour

There is clear evidence of open system behaviour from fission tracks, micro-milling and whole coral analyses. The difference between low and high [U] can be reduced over time, bioeroded surfaces are associated with extremely high [U] and whole coral analyses can return elevated $\delta^{234}U_{initial}$. In the following discussion we investigate the effects of adding uranium via three distinct mechanisms. The first two of these mechanisms add ^{238}U and ^{234}U with a $\delta^{234}U$ of 146.5 ‰ and are given by the fluxes FX^{pptn} and FX^{org}. FX^{pptn} is U added in areas that were precipitated with a distribution coefficient lower than 1 and FX^{org} is U added by bioerosion. The third mechanism adds only ^{234}U, and is a direct extension of the process of preferential movement of $^{234}U^{AR}$. Adding uranium to the system during diagenesis will lead to inaccurate ages, and if it is not homogeneous addition it will also cause isotopic heterogeneity.

When the coral calcifies it controls the [U] of the aragonite, so the [U] variability can be considered to be a "vital effect". We assume that the low [U] central band of the coral is precipitated out of thermodynamic equilibrium with a Kd<1 and that FX^{pptn} acts to redress this disequilibrium. FX^{pptn} leads to a reduction in the difference between the maximum and minimum [U], consistent with our fission track data and could be the result of secondary precipitation or re-mineralisation. We model FX^{pptn} as a U-flux (f_{pptn}) that is scaled to the difference between $U/Ca_{seawater}$ and $U/Ca_{aragonite}$ assuming that the process moves towards a $Kd_{inorganic}$ of 1:

$$FX^{pptn} = f_{pptn}(Kd_{inorganic} - Kd_{coral}) \quad \text{(Equation 6)}$$

If the uranium is added continually over the diagenetic history of the coral, then $\delta^{234}U_{initial}$ gradients can develop, giving elevated $\delta^{234}U_{initial}$ in zones that started with low [U] (Figure 11c). However the

maximum change of ~2 ‰ at 20 ka and 7 ‰ at 200 ka is much lower than the typical changes observed in the data (Figure 7). If this addition occurs rapidly after coral formation, there is even less effect on the $\delta^{234}U_{initial}$.

The second mechanism for U-addition is by bioerosion. We observe numerous endolithic sponge borings in fossil deep-sea corals that leave a brown coloured residue probably containing organic matter (Figure 7). Organic matter can have a [U] of up to 70ppm *[Amiel et al.*, 1973] so even 1% residual organic matter can cause >20% increase in the measured [U]. The important distinction between the total U-flux from bioerosion and secondary precipitation is that the final [U] can reach much greater values in the former case. Since the timing of bioerosion is unknown a continuous flux from organic matter, FX^{org}, is added to the two outermost boxes, with $FX^{org}/2$ to the two adjacent interior boxes, and this U is not permitted to move through the coral. Adding a [U] flux of $1x10^{-12}$ mol/yr (20 ka) and $1x10^{-13}$ mol/yr (200 ka) generates concentrations of ~8 ppm, with corresponding $\delta^{234}U_{initial}$ values of ~148 ‰ and ~169 ‰ respectively. However, the elevated $\delta^{234}U_{initial}$ zones are associated with high [U] (Figure 11d) and so are in direct contrast to the observations (Figure 8). Whole coral $\delta^{234}U_{initial}$ values reach only 147 ‰ and 154 ‰. Adding uranium through this mechanism causes the apparent calculated ages to be younger than the "real" age since the ($^{230}Th/^{238}U$) is reduced by the addition of ^{238}U. For these two model runs we calculate apparent ages of 18.6 ka and 179 ka, an inaccuracy of ~ 7 % and 11 % from the true ages.

Adding uranium with a $\delta^{234}U$ of 146.5 ‰ over time is certainly a potential mechanism for producing elevated $\delta^{234}U_{initial}$ values in fossil corals, but, even in the extreme case of 100% replacement of the primary uranium at the time of collection, U-addition cannot account for the full extent of $\delta^{234}U_{initial}$ elevations observed in those corals whose measured $\delta^{234}U$ lies above the modern seawater value (Figure 1).

In the two septal samples that display elevated $\delta^{234}U_{initial}$, (16 ka and 218 ka) we observe that the outer edges are not as depleted in $\delta^{234}U_{initial}$ as we would expect from allowing preferential movement of $^{234}U^{AR}$ through the coral. This observation indicates that there is an external source of ^{234}U to the edges. Both direct transfer of alpha-recoil products and preferential movement of $^{234}U^{AR}$ cause net transfer of isotopes across [U] gradients, so a potential source of ^{234}U to the coral is from a high [U] surface layer. Most fossil corals are coated in a thin black/brown ferromanganese layer, but this coating is not a likely source of ^{234}U since it has a ^{238}U concentration of only ~3 ppm, similar to the aragonite itself [*Cheng et al.*, 2000a]. However, if a thin veneer of U-rich organic matter is trapped between the coral and the ferromanganese coating it may provide such a source. We model this process by adding an extra box to either end of our model with a [U] of 6ppm and then allowing preferential movement of $^{234}U^{AR}$, at the same rate as the acicular aragonite. We then calculate an age and $\delta^{234}U_{initial}$ for the coral from all except the outermost high [U] coating. This "sampling" is done to mimic the physical cleaning procedure that abrades the exterior surface from the real corals. The model results are, of course, similar to the $^{234}U^{AR}$ movement modelled in the previous section (Figure 9b) but the edges have a higher $\delta^{234}U_{initial}$. The final whole coral $\delta^{234}U_{initial}$ values of 147 ‰ (20ka) and 164 ‰ (200ka) are associated with ages that are less than 0.5 % younger than the "real" age. Preferential movement of $^{234}U^{AR}$ from a high [U] coating can cause whole coral $\delta^{234}U_{initial}$ elevations with minimal changes to the model age.

Three corals exhibit $\delta^{234}U_{initial}$ values that are higher than seawater, and therefore must have experienced some open system behaviour. In the following discussion we test how a combination of closed and open system processes may produce the observed isotopic patterns, and how this diagenesis may affect the final apparent age of each sample. One difficulty in this modelling is setting the initial [U] boundary conditions if uranium is being added over time. The fission track

data shows that the contrast between the minimum and maximum [U] is reduced from a factor of >3 to ~2 over 33 ka, but we do not know how rapidly this process takes place. In all micro-milled samples from modern back to 218 ka this contrast is approximately a factor of 2, which reflects, in part, the inherent bias when micro-sampling across several 100s μm, but may also reflect early U-addition. Surface coral studies have shown rapid diagenetic pathways for U *[Swart & Hubbard*, 1982] so we assume that U-addition takes place soon after death and use the measured [U] concentrations for setting the initial boundary conditions.

The 11 ka coral has clearly been bioeroded and has associated [U] concentrations of up to 15 ppm (Figure 6). The samples next to the high [U] zone have the highest $\delta^{234}U_{initial}$, suggesting that the bioerosion occurred early in the post-mortem history as there has been sufficient time for $^{234}U^{AR}$ to move down through the coral from the high [U] area (Figure 10c). We use the internal reorganisation processes described in Equations 2-5 to model the 11ka coral and produce an isotopic pattern consistent with the observations (Figure 12c). The discrepancy between the modelled and real data seen in Figure12c is due to the fact that there is no late U-addition and so no whole coral $\delta^{234}U_{initial}$ elevation. This discrepancy may be caused by a second boring, characterised by a brown stain, which cuts straight across the base of the section that we sub-sampled (Figure 2). This surface is a potential source of $^{234}U^{AR}$ atoms that may have a net transfer into the rest of the coral causing the observed whole coral $\delta^{234}U_{initial}$ elevation.

The last two corals (16 ka and 218 ka) are both septal samples, and have no evidence for bioerosion. However elevated $\delta^{234}U_{initial}$ with no associated [U] increase at the outer edges of both corals suggests an external source of ^{234}U, so in each case we add a high [U] coating (Figure 12d and 12e). Again we use the processes described in Equation 2-5 to model these two corals. Both model runs produce spatial patterns and $\delta^{234}U_{initial}$ ranges that are similar to the observations. The

whole coral model $\delta^{234}U_{initial}$ elevations of 149 ‰ and 165 ‰ for the two corals are similar to the observed values of 153 ‰ and 161 ‰. The associated model ages for the 16 ka and 218 ka coral are only ~ 0.1 % and 1.0 % different from the closed-system ages respectively.

The differences between real and modelled whole coral $\delta^{234}U_{initial}$ values and the discrepancies in the spatial patterns across coral sections may be due to a number of simplifications made in the model. We assume uniform diffusion constants for $^{234}U^{AR}$ in each crystal type, but the presence of micro-cracks and/or micro- pore waters is likely to cause heterogeneity. Our [U] initial boundary condition is based on micro-milling at a ~100μm scale, but the fission-track data shows us that [U] variability is present on a much finer scale. The exact [U] distribution is extremely important in determining the net ^{234}U transfer between sub-samples. Small adjustments to the fine scale [U] distribution and rate constants would allow us to tune our model results to be identical to the observations.

This study has used deep-sea scleractinian corals, but surface corals also have primary [U] gradients, are subject to bioerosion and display a similar whole-coral U-Th isotopic distribution (Figure 1). The processes described in this model are, therefore, likely to be important for surface corals, particularly for those samples that have spent most of their diagenetic history submerged in seawater [*Bard et al.*, 1990b; *Toscano & Lundberg*, 1999]. Without a detailed knowledge of the U-Th distribution within a specific sample it is not, however, possible to convert closed-system ages to open-system ages

Conclusions

The presence of [U] heterogeneity within carbonates can lead to the development of large isotopic gradients. The physical processes that cause these gradients are direct transfer of alpha-recoil ^{230}Th

and ^{234}Th and, more importantly, preferential movement of alpha-decay produced ^{234}U. Internal, closed-system processes cannot alter the apparent age or $\delta^{234}U_{initial}$ unless coupled with a sampling bias. Such biases may be the removal of bioeroded material or of the surface layers of the coral. If the surface has a high [U] coating then preferential movement of alpha-decay produced ^{234}U can lead to large whole-coral $\delta^{234}U_{initial}$ elevations with little change to the apparent age. By contrast, addition of both ^{238}U and ^{234}U gives smaller $\delta^{234}U_{initial}$ elevations with large age inaccuracies.

REFERENCES

Adkins J. F., E. A. Boyle, W. B. Curry and A. Lutringer. (2003) Stable isotopes in deep-sea corals and a new mechanism for "vital effects". *Geochim. Cosmochim. Acta* 67(6), 1129-1143.

Adkins J. F., H. Cheng, E. A. Boyle, E. R. M. Druffel and R. L. Edwards. (1998) Deep-sea coral evidence for rapid change in ventilation of the deep North Atlantic 15,400 years ago. *Science* 280(5364), 725-728.

Adkins J. F., G. M. Henderson, S. L. Wang, S. O'Shea and F. Mokadem. (2004) Growth rates of the deep-sea scleractinia Desmophyllum cristagalli and Enallopsammia rostrata. *Earth and Planetary Science Letters* 227(3-4), 481-490.

Amiel A. J., D. S. Miller and G. M. Friedman. (1973) Incorporation of uranium in modern corals. *Sedimentology* 20, 523-528.

Bard E., R. G. Fairbanks, B. Hamelin, A. Zindler and H. Chi Trach. (1991) Uranium-234 anomalies in corals older than 150 000 years. *Geochim. Cosmochim. Acta* 55(8), 2385-2390.

Bard E., B. Hamelin and R. G. Fairbanks. (1990a) U-Th ages obtained by mass spectrometry in corals from Barbados: sea level during the past 130 000 years. *Nature* 346(6283), 456-458.

Bard E., B. Hamelin, R. G. Fairbanks and A. Zindler. (1990b) Calibration of the C-14 timescale over the past 30 000 years using mass spectrometric U-Th ages from Barbados corals. *Nature* 345(6274), 405-409.

Bender M. L., R. G. Fairbanks, F. W. Taylor, R. K. Matthews, J. G. Goddard and W. S. Broecker. (1979) Uranium-series dating of the Pleistocene reef tracts of Barbados, West Indies. *Geological Society of America Bulletin* 90(6), I 577-I 594.

Broecker W., S. (1963) Preliminary evaluation of uranium series inequilibrium as a tool for absolute age measurement on marine carbonates. *Journal of Geophysical Research* 68(9), 2817-2834.

Broecker W., S. and T. Takahashi. (1966) Calcium carbonate precipitation on the Bahama Banks. *Journal of Geophysical Research* 71(6), 1575-1602.

Cheng H., J. Adkins, R. L. Edwards and E. A. Boyle. (2000a) U-Th dating of deep-sea corals. *Geochim. Cosmochim. Acta a* 64(1-4), 2401-2416.

Cheng H., R. L. Edwards, J. Hoff, C. D. Gallup, D. A. Richards and Y. Asmeron. (2000b) The half-lives of uranium-234 and thorium-230. *Chemical Geology* 169, 17-33.

Cherniak D. J. (1997) An experimental study of strontium and lead diffusion in calcite, and implications for the carbonate diagenesis and metamorphism. *Geochim. Cosmochim. Acta* 61, 4173-4179.

Cutler K. B., R. L. Edwards, F. W. Taylor, H. Cheng, J. Adkins, C. D. Gallup, P. M. Cutler, G. S. Burr and A. L. Bloom. (2003) Rapid sea-level fall and deep-ocean temperature change since the last interglacial period. *Earth and Planetary Science Letters* 206(3-4), 253-271.

Djogic R., G. Kniewald and M. Branica. (1987) Uranium in the marine environment; a geochemical approach to its hydrologic and sedimentary cycle. *Radioact. Oceangr*, 171-182.

Edwards R. L., J. H. Chen and G. J. Wasserburg. (1986) 238U-234U-230Th-232Th systematics and the precise measurement of time over the past 500 000 years. *Earth and Planetary Science Letters* 81(2-3), 175-192.

Edwards R. L., H. Cheng, M. T. Murrell and S. J. Goldstein. (1997) Protactinium-231 dating of carbonates by thermal ionization mass spectrometry: implications for Quaternary climate change. *Science* 276(5313), 782-786.

Fleischer R. L. (1988) Alpha-recoil damage: relation to isotopic disquilibrium and leaching of radionuclides. *Geochim. Cosmochim. Acta* 52(6), 1459-1466.

Frank N., M. Paterne, L. Ayliffe, T. van Weering, J. P. Henriet and D. Blamart. (2004) Eastern North Atlantic deep-sea corals: tracing upper intermediate water Delta C-14 during the Holocene. *Earth and Planetary Science Letters* 219(3-4), 297-309.

Gallup C. D., R. L. Edwards and R. G. Johnson. (1994) The timing of high sea levels over the past 200 000 years. *Science* 263(5148), 796-800.

Goldstein S. J., D. W. Lea, S. Chakraborty, M. Kashgarian and M. T. Murrell. (2001) Uranium-series and radiocarbon geochronology of deep-sea corals: Implications for Southern Ocean ventilation rates and the oceanic carbon cycle. *Earth and Planetary Science Letters* 193(1-2), 167-182.

Henderson G. M. (2002) Seawater ($^{234}U/^{238}U$) during the last 800 thousand years. *Earth and Planetary Science Letters* 199(1-2), 97-110.

Henderson G. M., N. C. Slowey and M. Q. Fleisher. (2001) U-Th dating of carbonate platform and slope sediments. *Geochim. Cosmochim. Acta* 65(18), 2757-2770.

Kigoshi K. (1971) Alpha-recoil thorium-234; dissolution into water and the uranium-234/ uranium-238 disequilibrium in nature. *Science* 173(3991), 47-48.

Lazar B., R. Enmar, M. Schossberger, M. Bar-Matthews, L. Halicz and M. Stein. (2004) Diagenetic effects on the distribution of uranium in live and Holocene corals from the Gulf of Aqaba. *Geochim. Cosmochim. Acta a* 68(22), 4583-4593.

Lazier A. V., J. E. Smith, M. J. Risk and H. P. Schwarcz. (1999) The skeletal structure of Desmophyllum cristagalli: the use of deepwater corals in sclerochronology. *Lethaia* 32(2), 119-130.

Li Y. H. and S. Gregory. (1974) Diffusion of ions in sea water and in deep-sea sediments. *Geochim. Cosmochim. Acta* 38, 703-714.

Lomitschka M. and A. Mangini. (1999) Precise Th/U-dating of small and heavily coated samples of deep sea corals. *Earth and Planetary Science Letters* 170(4), 391-401.

Min G. R., R. L. Edwards, F.W. Taylor, J. Recy, C.D. Gallup and J. W. Beck. (1995) Annual cycles of U/ Ca in coral skeletons and U/ Ca thermometry. *Geochim. Cosmochim. Acta* 59(10), 2025-2042.

Murrell M. T. and D. S. Burnett. (1982) Actinide Microdistributions in the Enstatite Meteorites. *Geochim. Cosmochim. Acta* 46(12), 2453-2460.

Pingitore N. E., A. Iglesias, F. Lytle and G. M. Wellington. (2002) X-ray absorption spectroscopy of uranium at low ppm levels in coral skeletal aragonite. *Microchemical Journal* 71(2-3), 261-266.

Reeder R. J., M. Nugent, C. D. Tait, D. E. Morris, S. M. Heald, K. M. Beck, W. P. Hess and A. Lanzirotti. (2001) Coprecipitation of Uranium(VI) with Calcite: XAFS, micro-XAS, and luminescence characterization. *Geochim. Cosmochim. Acta* 65(20), 3491-3503.

Robinson L. F., J. F. Adkins, L. D. Keigwin, J. Southon, D. P. Fernandez, S. L. Wang and D. S. Scheirer. (submitted) Radiocarbon variability in the Western North Atlantic during the last deglaciation. *Science*.

Robinson L. F., N. S. Belshaw and G. M. Henderson. (2004a) U and Th concentrations and isotope ratios in modern carbonates and waters from the Bahamas. *Geochim. Cosmochim. Acta* 68(8), 1777-1789.

Robinson L. F., G. M. Henderson, L. Hall and I. Matthews. (2004b) Climatic control of riverine and Seawater uranium-isotope ratios. *Science* 305(5685), 851-854.

Russell A. D., B. Honisch, H. J. Spero and D. W. Lea. (2004) Effects of seawater carbonate ion concentration and temperature on shell U, Mg, and Sr in cultured planktonic foraminifera. *Geochim. Cosmochim. Acta* 68(21), 4347-4361.

Scholz D., A. Mangini and T. Felis. (2004) U-series dating of diagenetically altered fossil reef corals. *Earth and Planetary Science Letters* 218(1-2), 163-178.

Schroeder J. H., D. S. Miller and G. M. Friedman. (1970) Uranium distribution in recent skeletal carbonates. *Journal of Sedimentary Petrology* 40, 672-681.

Shen G. T. and R. B. Dunbar. (1995) Environmental Controls on Uranium in Reef Corals. *Geochimica Et Cosmochimica Acta* 59(10), 2009-2024.

Smith J. E., H. P. Schwarcz, M. J. Risk, T. A. McConnaughey and N. Keller. (2000) Paleotemperatures from deep-sea corals: Overcoming 'vital effects'. *Palaios* 15(1), 25-32.

Stirling C. H., T. M. Esat, M. T. McCulloch and K. Lambeck. (1995) High-precision U-series dating of corals from Western Australia and implications for the timing and duration of the last interglacial. *Earth and Planetary Science Letters* 135(1-4), 115-130.

Swart P. K. and J. A. E. B. Hubbard. (1982) Uranium in scleractinian coral skeletons. *Coral Reefs* 1, 13-19.

Szabo B. J., K. R. Ludwig, D. R. Muhs and K. R. Simmons. (1994) Thorium-230 ages of corals and duration of the last interglacial sea-level high stand on Oahu, Hawaii. *Science* 266(5182), 93-96.

Thompson W. G. and S. L. Goldstein. (2005) Open-system coral ages reveal persistent suborbital sea-level cycles. *Science* 308(5720), 401-404.

Thompson W. G., M. W. Spiegelman, L. Goldstein Steven and Speed Robert C. (2003) An open-system model for U-series age determinations of fossil corals. *Earth and Planetary Science Letters* 210, 365-381.

Toscano M. A. and J. Lundberg. (1999) Submerged late pleistocene reefs on the tectonically-stable S.E. Florida margin: High-precision geochronology, stratigraphy, resolution of substage 5a sea-level elevation, and orbital forcing. *Quaternary-Science-Reviews. 1999; 18(6): 753-767* 18(6), 753-767.

Villemant B. and N. Feuillet. (2003) Dating open systems by the U-238-U-234-Th-230 method: application to Quaternary reef terraces. *Earth and Planetary Science Letters* 210(1-2), 105-118.

FIGURES

Figure 1: Comparison of measured deep-sea (diamonds) and surface coral (crosses) ($^{234}U/^{238}U$) and ($^{230}Th/^{238}U$) values. Deep-sea coral data are from this study (Table 1), and surface coral data are from *[Bard et al.*, 1990a; *Bard et al.*, 1990b; *Szabo et al.*, 1994; *Cutler et al.*, 2003; *Thompson et al.*, 2003]. The solid grey line shows the isotopic evolution of a closed system starting with a ($^{234}U/^{238}U$) of 1.1465 and a ($^{230}Th/^{238}U$) of zero. Deviations from this line are symptomatic of diagenetic alteration from a closed system. The dashed line is at the modern seawater ($^{234}U/^{238}U$) activity ratio and any points that fall above it cannot be explained by diagenetic addition of U with the seawater ($^{234}U/^{238}U$) ratio only.

Figure 2: Figure 2 shows reflected light images of two corals sections. Figure 2a is a thecal section from an 11 ka coral. The irregularity and brown discoloration across the lower surface and at the upper right hand side are caused by endolithic boring. Figure 2b is a section through a septum of a 43 ka coral. The black lines delimit the sampling done by micro-milling, which aimed to follow the visible banding (Figure 3). The nature of the micro-milling means that some slices sampled both dark and light coloured areas.

Figure 3: The four images show the banding present in *D dianthus*. Figure 3a is an SEM image of an etched thin section of a coral septum. The central band (aligned vertically) is filled by irregular fine grained aragonite (gr), which is surrounded by elongated acicular crystals (ac). In the central band there are two dark coloured features which have the appearance of collapsed spheres (labelled sp). The longitudinal ridges across the acicular crystals are thought to be caused by preferential dissolution, perhaps due to the variable organic or Mg content. The blow up in Figure 3b depicts an un-treated fractured surface and highlights the difference between these two crystal morphologies. Figure 3c is a petrographic image from a thecal section. The two dark lines are equivalent to the single central band in the septal images, and their optical density may be due to the presence of

multiple organic “spheres” integrated through the thickness of the section. The acicular crystals are clearly arranged in bunches aligned along their c-axis. Figure 3d is a transmitted light image of a coral septum and clearly shows light and dark banding.

Figure 4: Two images of the same coral section compare the visible and fission-track banding. Figure 4a shows the visible banding viewed though a transmitting light microscope. Figure 4b is a reflected light image of the mica used to record the density of fission tracks generated by neutron bombardment. The dark areas have few fission tracks relative to the light areas. The fission track density is directly proportional to the [^{235}U] which is, in turn, directly proportional to the [^{238}U]. These two images highlight the similarity between visible banding and [U], even in areas characterised by detailed variability.

Figure 5: Figure 5a shows a fission-track density profile overlying the transmitted light image of the visible banding and is a blow up of Line 3 in Figure 6. The lowest [U] runs through the centre of the septa, but is wider than visible banding, indicating that the dark part of the visible banding does not control the U distribution.

Figure 6: The two panels show visible banding (left), fission track density image (right) and four plots of relative [U] for (a) a modern coral and (b) a 33 ka fossil coral. The fossil sample shows a significantly reduced contrast between high and low [U] bands (< factor of 2) compared to the modern coral (> factor of 3), but the detailed structure of the U-heterogeneity is retained.

Figure 7: Histograms showing the age and number distribution of [U] in whole coral samples analysed to determine the ages (Table 1). Black bars show all samples including replicates, grey bars exclude replicates. Figure 7a shows the average [U] for corals in discrete time slices over the last 300 ka. Figure 7b shows the number of corals in [U] 0.2 ppm divisions.

Figure 8: U concentration (ppm) plotted against $\delta^{234}U_{initial}$ (‰) for all deep sea corals analysed in this study. Uncertainties are 2 s.e. for $\delta^{234}U_{initial}$ and are within the symbol size for [U]. Figure 8a compares analyses made on whole chunks of coral (Table 2) to the micro-milled slices in Table 1. The similarity of the two distributions is suggestive of the same processes being responsible on both 0.1-10mm scales. Figures 8b and c show the micro-milled data in more detail. Figure 8b displays the individual measurements of corals of 11 ka, 15 ka and 16 ka together with the modern coral plotted as the total range of [U] and the average $\delta^{234}U_{initial}$ with a 2 s.d. range. Figure 8c shows the distribution in the oldest three corals, 43 ka, 83 ka and 218 ka. In all cases the dashed horizontal line represents the modern seawater value. The half lives used to calculate activities are from ^{230}Th and ^{234}U are from [*Cheng et al.*, 2000b].

Figure 9: Arranged in order of increasing age, Figures 9a-e show the measured spatial distribution of $\delta^{234}U_{initial}$ and [U] for five different corals. Error bars for $\delta^{234}U_{initial}$ are 2 s.e. Starred [U] sub-samples may have lost powder whilst transferring from weighing to dissolution vials, and therefore will have an inaccurate, low [U].

Figure 10: Schematic diagram of initial boundary conditions and processes for the model sensitivity study shown in Figure 9. The model is divided into 25 boxes of 50 μm width. The central three boxes, shaded light grey, represent fine grained irregular aragonite and the white boxes represent the acicular crystals. The outermost dark grey area is representative of a high (6 ppm) [U] coating, such as an organic film. In addition to radioactive decay we model five processes, bioerosion, secondary precipitation, "diffusion", direct transfer of alpha-recoil ^{230}Th and ^{234}Th and

preferential movement of alpha-decay mobilised ^{234}U. ^{230}Th is not subject to preferential movement because Th is much less mobile than U in this type of environment.

Figure 11: Four model scenarios run for 20 ka (diamonds, right hand axes) and 200 ka (triangles, left hand axes) demonstrate the sensitivity of $\delta^{234}U_{initial}$ and age for each of the processes described in the text and shown in Figure 10. The model results are displayed as $\delta^{234}U_{initial}$ versus [U] to allow comparison with the measurements shown in Figure 8. The separate plots show (a) direct transfer of ^{230}Th and ^{234}Th by alpha recoil (b) preferential movement of alpha-decay produced ^{234}U (c) secondary precipitation and (d) addition of U by bioerosion

Figure 12: Application of the U-diagenesis model to the five corals shown in Figure 6. Grey and white areas in the schematic coral sections represent areas of granular and acicular aragonite respectively. Heavy lines delimit the physical sampling of the coral. Black bars on 10d and e represent high [U] coatings. Black crosses are data with 2 s.e. error-bars which are smaller than the symbol size for [U]. Grey diamonds in each of the upper plots are the model output using the [U] boundary conditions shown by the grey line in the lower plot. In all five cases the only processes being modelled are radioactive decay, direct transfer of ^{230}Th and ^{234}Th by alpha recoil and preferential movement of alpha-decay mobilised ^{234}U.

Table 1: Micro-sampled U-series results from seven coral sections, ranging from modern to 218 ka. For each coral the sample name, age and integrated $\delta^{234}U_{initial}$ values are tabulated. For each sub sample the approximate width in microns are shown. Samples marked with a # targeted discrete areas within coral sections and so are not suited to modelling the evolution of the U-series isotopes. All errors are 2s.e. Starred [U] sub-samples may have lost powder whilst transferring from weighing to dissolution vials, and therefore will have an inaccurate, low [U].

	Width	Weight	[U]		$\delta^{234}U_{meas}$		$\delta^{234}U_{initial}$ (‰)	
	μm	mg	ppm		‰		‰	
47407								
Age (ka)	Modern							
47_Ba.1	2000	0.935	5.27	0.11	140.0	2.0	140.0	2.0
47_Ba.2	875	1.085	5.02	0.09	141.0	2.1	141.0	2.1
47_Ba.3	388	1.020	2.82	0.06	143.7	2.6	143.7	2.6
47_Ba.4	375	1.917	3.07	0.03	145.0	2.2	145.0	2.2
47_Ba.5	88	0.799	3.63	0.09	143.7	2.6	143.7	2.6
47_Ba.6	100	0.631	3.80	0.12	146.6	2.5	146.6	2.5
47_Ba.7	125	0.690	3.23	0.09	146.5	3.5	146.5	3.5
JFA 39 B								
Age (ka)	14.80	0.10						
$\delta^{234}U_{initial}$ (‰)	146.93	1.21						
39_B.1	360#	0.324	6.21	0.38	145.9	4.1	152.1	4.4
39_B.2	280#	0.300	3.76	0.25	148.7	4.6	155.0	4.8
39_B.3	360#	1.590	3.70	0.05	148.1	1.9	154.4	2.0
39_B.4	800#	2.885	3.08	0.02	156.7	2.4	163.4	2.6
37_2								
Age (ka)	10.96	0.10						
$\delta^{234}U_{initial}$ (‰)	148.85	1.09						
37_2_Ba.1	#	0.662	2.02	0.06	154.8	4.4	159.7	4.6
37_2_Ba.2	#	0.810	4.28	0.11	144.8	1.8	149.3	1.9
37_2_Ta.1	#	1.120	2.79	0.05	145.9	2.7	150.5	2.8
37_2_Ta.2	533	1.706	4.44	0.05	141.7	1.4	146.2	1.4
37_2_Ta.3	233	0.660	3.59	0.11	144.1	3.4	148.6	3.5
37_2_Ta.4	167	2.225	4.58	0.04	143.2	1.3	147.7	1.4
37_2_Ta.5	800	3.434	2.47	0.01	148.0	1.6	152.6	1.7
37_2_Ta.6	300	1.818	6.95	0.08	147.6	1.9	152.3	2.0
37_2_Ta.7	200	0.496	14.99	0.60	144.0	2.6	148.5	2.8
37_2_Ta.8	200	0.639	2.38	0.07	149.8	4.9	154.5	5.1
ALV-3892-1315-001-008								
Age (ka)	16.15	0.14						
$\delta^{234}U_{initial}$ (‰)	149.08	1.13						
A	150	1.691	4.80	0.11	146.2	3.5	153.0	3.7
B	200	1.308	3.25	0.10	145.3	4.5	152.1	4.8
C	150	0.788	2.73	0.14	152.4	5.5	159.5	5.8
D*	200	1.307	1.91	0.06	148.2	5.2	155.1	5.5
E	350	2.615	2.95	0.05	141.1	3.4	147.7	3.7
F	200	0.950	3.52	0.15	144.7	4.2	151.5	4.4
G	250	0.720	4.74	0.26	147.0	4.7	153.9	5.0
ALV-3892-1421-002-001-14								
Age (ka)	43.87	0.34						
$\delta^{234}U_{initial}$ (‰)	144.50	4.54						

W	154	0.930	5.20	0.22	124.0	4.6	140.3	5.4
X	231	1.500	4.18	0.11	125.8	3.3	142.4	3.9
Y	231	1.230	3.30	0.11	124.5	4.6	140.9	5.3
Z	115	1.000	2.57	0.10	127.0	5.6	143.8	6.4
AA	192	1.000	2.69	0.11	136.9	5.2	154.9	6.0
BB	231	1.320	2.96	0.09	135.1	5.0	153.0	5.8
CC	231	1.140	4.78	0.17	125.5	4.2	142.1	5.0
ALV-3887-1436-003-007								
Age (ka)	83.03	2.83						
$\delta^{234}U_{initial}$ (‰)								
P*	148	0.720	3.65	0.20	112.9	6.7	142.7	9.6
Q	148	1.170	3.79	0.13	112.9	3.8	142.7	6.0
R	148	1.060	4.07	0.15	119.9	4.0	151.6	6.3
S	148	0.950	3.46	0.15	129.0	5.3	163.1	8.1
T	111	0.920	3.50	0.15	108.4	4.4	137.1	6.7
U*	148	1.300	2.70	0.08	112.4	5.0	142.2	7.5
V	185	1.460	2.62	0.07	109.7	4.6	138.7	6.9
ALV-3889-1326-002-B7								
Age (ka)	218.49	4.00						
$\delta^{234}U_{initial}$ (‰)	152.3	2.75						
H	200	0.960	5.56	0.23	83.4	3.4	154.6	8.2
I	200	1.410	4.52	0.13	81.0	4.7	150.2	10.5
J	200	1.510	3.34	0.09	82.0	4.9	152.1	11.0
K	200	1.190	2.40	0.08	95.0	5.1	176.1	11.5
L	150	0.990	2.57	0.10	119.1	6.7	220.8	15.0
M	150	1.100	2.27	0.08	93.5	7.5	173.4	16.0
N	250	1.110	2.62	0.09	82.4	4.3	152.7	9.7
O	250	0.960	3.04	0.13	82.8	4.1	153.6	9.4

Table 2: Uranium series data summary of concentrations and isotopic ratios from pieces of coral, referred to as "whole" coral analyses in text. All errors are 2 σ. Calculated ages are reported before and after correction for $^{230}Th_{initial}$ correction, and are in years before date of analysis (2004).

Lab ID	Database ID	^{238}U (ppm)		^{230}Th (ppt)		^{232}Th (ppb)		$\delta^{234}U_{initial,\ raw}$ (‰)		$(^{232}Th/^{238}U)_{act}$		Age_{raw} (yrs)		Age_{corr} (yrs)		$\delta^{234}U_{initial,\ corr}$ (‰)	
UAA7	ALV-3883-1248-003-004	3.531	0.008	22.57	0.10	5.148	0.023	129.39	2.03	0.3834	0.0072	45928	301	44891	1051	146.9	2.3
UAA1	ALV-3883-1346-004-003	3.836	0.008	26.37	0.12	8.757	0.038	127.10	2.02	0.4088	0.0110	50420	333	48736	1660	145.9	2.4
UAE11	ALV-3884-1411-002-104	3.199	0.002	8.28	0.04	1.659	0.007	142.59	1.10	0.1555	0.0027	16218	79	15925	296	149.2	1.2
UAF08	ALV-3884-1531-002-013	3.383	0.002	8.42	0.04	0.339	0.011	140.17	1.09	0.1516	0.0008	15586	75	15530	92	146.5	1.1
UAJ17	ALV-3884-1531-003-008	3.700	0.004	9.25	0.04	2.202	0.016	145.48	1.20	0.1497	0.0030	15579	79	15245	333	151.9	1.3
UAE12	ALV-3884-1638-004-210	3.286	0.002	8.16	0.04	0.422	0.002	141.65	1.19	0.1511	0.0009	15532	75	15458	103	148.0	1.2
UAI02	ALV-3885-1239-001-002	3.507	0.003	10.00	0.05	9.195	0.043	145.25	1.09	0.1608	0.0124	17955	102	16471	1370	152.2	1.3
UAG15	ALV-3885-1239-001-004	3.416	0.002	9.10	0.04	1.602	0.625	142.20	1.11	0.1604	0.0024	16733	84	16476	263	149.0	1.2
UAE10	ALV-3885-1239-001-007	3.129	0.002	8.47	0.04	3.092	0.013	146.45	1.11	0.1604	0.0049	16963	82	16405	544	153.4	1.2
UAO17	ALV-3885-1239-001-007	3.135	0.002	7.99	0.04	0.701	0.011	146.73	1.07	0.1547	0.0013	15899	80	15777	142	153.4	1.1
UAG08	ALV-3885-1239-001-011	2.289	0.002	5.99	0.03	0.672	0.989	140.59	1.14	0.1584	0.0016	16438	82	16277	176	147.2	1.2
UAI03	ALV-3885-1239-001-012	3.087	0.002	8.16	0.04	1.795	0.010	142.12	1.11	0.1586	0.0030	16607	92	16277	333	148.8	1.2
UAO18	ALV-3885-1239-001-012	3.317	0.002	8.43	0.04	0.888	0.010	150.62	1.06	0.1539	0.0015	15779	79	15634	161	157.4	1.1
UAE06	ALV-3885-1239-001-014	4.829	0.002	12.63	0.05	1.116	0.005	142.41	1.11	0.1586	0.0014	16401	79	16268	151	149.1	1.2
UAG11	ALV-3885-1239-001-015	3.384	0.002	8.81	0.04	0.735	1.214	141.63	1.11	0.1581	0.0013	16343	83	16223	141	148.3	1.2
UAF09	ALV-3885-1420-003-003	3.634	0.002	27.95	0.12	1.203	0.009	121.61	1.11	0.4682	0.0026	58615	343	58339	431	143.4	1.3
UAG16	ALV-3885-1739-007-003	2.693	0.002	42.33	0.19	3.676	0.477	96.94	1.14	0.9536	0.0079	212243	2911	207902	5063	174.5	3.2
UAJ20	ALV-3887-1324-002-005	4.596	0.004	9.34	0.04	0.572	0.009	140.89	1.13	0.1235	0.0009	12552	63	12483	92	145.9	1.2
UAI16	ALV-3887-1436-003-003	3.488	0.003	8.65	0.04	0.657	0.010	143.48	1.14	0.1506	0.0012	15486	78	15378	130	149.9	1.2
UAJ04	ALV-3887-1549-004-002	3.755	0.003	9.31	0.04	0.472	0.005	142.08	1.11	0.1507	0.0009	15486	77	15413	104	148.4	1.2
UAK02	ALV-3887-1549-004-004	3.470	0.003	9.01	0.04	0.533	0.009	143.34	1.08	0.1579	0.0010	16270	79	16181	117	150.1	1.1
UAF13	ALV-3887-1549-004-006	3.812	0.002	9.70	0.04	0.925	0.010	139.21	1.11	0.1544	0.0014	15986	77	15853	150	145.6	1.2
UAL19	ALV-3887-1549-004-006	3.922	0.005	10.07	0.04	1.609	0.009	136.27	1.33	0.1548	0.0022	16181	81	15947	242	142.6	1.4
UAF11	ALV-3887-1549-004-007	4.039	0.002	8.36	0.04	0.584	0.008	139.56	1.10	0.1258	0.0009	12822	61	12744	96	144.7	1.1
UAF12	ALV-3887-1549-004-008	4.282	0.002	10.55	0.05	0.592	0.009	148.27	1.03	0.1499	0.0009	15303	73	15227	103	154.8	1.1
UAI17	ALV-3887-1549-004-009	3.360	0.002	6.96	0.03	0.159	0.007	143.27	1.12	0.1264	0.0006	12787	63	12759	68	148.5	1.2
UAF02	ALV-3887-1549-004-012	3.286	0.002	6.76	0.03	0.561	0.012	142.53	1.10	0.1249	0.0010	12707	61	12616	107	147.7	1.1
UAA5	ALV-3887-1549-004-014	3.651	0.008	9.00	0.04	0.524	0.002	144.62	2.01	0.1499	0.0010	15358	86	15279	115	151.0	2.1
UAL09	ALV-3887-1549-004-014	3.644	0.002	8.99	0.04	0.327	0.007	147.28	1.09	0.1503	0.0008	15341	74	15289	89	153.8	1.1
UAA3	ALV-3887-1652-005-006	3.637	0.008	9.82	0.04	6.896	0.031	143.01	2.03	0.1557	0.0088	16970	96	15944	970	149.6	2.2
UAL12	ALV-3887-1652-005-006	3.480	0.001	7.16	0.03	0.385	0.004	142.45	1.10	0.1252	0.0008	12705	59	12643	84	147.6	1.1
UAF10	ALV-3887-1652-005-013	3.882	0.002	9.94	0.04	0.719	0.008	141.42	1.13	0.1555	0.0011	16042	77	15939	125	147.9	1.2
UAA4	ALV-3889-1311-001-006	3.262	0.007	14.24	0.06	3.179	0.014	134.03	2.02	0.2619	0.0049	29116	173	28519	605	145.3	2.2
UAL20	ALV-3889-1326-002-B7	3.048	0.002	47.76	0.21	2.142	0.011	82.14	1.16	0.9538	0.0055	221140	3172	218494	4005	152.3	2.7
UAA2	ALV-3889-1353-003-001	3.442	0.007	11.59	0.05	21.790	0.097	145.20	2.03	0.1747	0.0263	21531	128	18018	2977	152.8	2.5

Lab ID	Database ID	^{238}U (ppm)		^{230}Th (ppt)		^{232}Th (ppb)		$\delta^{234}U_{initial,\ raw}$ (‰)		$(^{232}Th/^{238}U)_{act}$		Age_{raw} (yrs)		Age_{corr} (yrs)		$\delta^{234}U_{initial,\ corr}$ (‰)	
UAL08	ALV-3889-1353-003-001	3.350	0.002	9.46	0.04	5.420	0.026	145.98	1.06	0.1642	0.0079	17752	87	16835	874	153.1	1.2
UAA8	ALV-3889-1526-006-001	3.890	0.008	55.57	0.25	26.959	0.118	102.20	2.02	0.8388	0.0328	164025	1990	150510	13029	156.4	6.7
UAE08	ALV-3889-1526-006-001	4.022	0.002	56.80	0.24	3.052	0.013	97.85	1.07	0.8589	0.0054	161549	1619	159899	2249	153.8	1.9
UAE03	ALV-3889-1526-006-B2	4.936	0.003	59.92	0.26	4.284	0.018	120.45	5.01	0.7373	0.0054	115159	1340	113946	1754	166.2	7.0
UAE04	ALV-3890-1235-001-002	3.522	0.002	20.52	0.09	1.019	0.004	139.19	5.01	0.3544	0.0021	40571	309	40361	366	156.0	5.6
UAG14	ALV-3890-1330-002-003	2.951	0.002	23.73	0.10	9.609	0.442	143.55	1.15	0.4754	0.0155	60488	375	57920	2496	169.1	1.8
UAG12	ALV-3890-1407-003-003	3.488	0.002	9.18	0.04	0.866	0.775	145.93	1.15	0.1596	0.0014	16467	83	16331	155	152.8	1.2
UAG13	ALV-3890-1407-003-003	3.579	0.002	9.42	0.04	2.138	0.564	143.23	1.13	0.1579	0.0030	16505	84	16181	326	149.9	1.2
UAE17	ALV-3890-1643-005-005	3.429	0.001	4.06	0.02	0.436	0.002	135.52	1.07	0.0718	0.0007	7187	35	7120	74	138.3	1.1
UAE05	ALV-3890-1718-006-001	3.267	0.004	2.36	0.01	2.132	0.009	149.63	5.02	0.0408	0.0031	4272	28	3944	304	151.3	5.1
UAE07	ALV-3890-1742-007-001	4.292	0.002	11.14	0.05	2.975	0.013	146.02	1.12	0.1550	0.0035	16215	78	15825	386	152.7	1.2
UAK20	ALV-3890-1742-007-002	3.039	0.002	8.06	0.04	0.982	0.009	148.39	1.10	0.1603	0.0018	16548	82	16365	196	155.4	1.2
UAI05	ALV-3891-1459-003-002	4.496	0.003	8.39	0.04	0.879	0.006	139.61	1.08	0.1131	0.0011	11493	56	11385	118	144.2	1.1
UAJ11	ALV-3891-1459-003-004	3.766	0.003	8.72	0.04	3.216	0.015	142.62	1.17	0.1370	0.0043	14388	75	13915	462	148.3	1.2
UAO19	ALV-3891-1459-003-009	3.605	0.002	9.36	0.04	0.665	0.015	157.02	1.07	0.1578	0.0011	16056	79	15955	124	164.3	1.1
UAL05	ALV-3891-1459-003-013	3.734	0.002	3.99	0.02	1.290	0.010	141.74	1.13	0.0636	0.0017	6430	30	6251	176	144.3	1.2
UAK16	ALV-3891-1546-004-003	3.582	0.003	3.27	0.01	5.174	0.024	147.52	1.07	0.0484	0.0064	5433	26	4701	635	149.5	1.1
UAA6	ALV-3891-1646-004-004	3.833	0.008	9.60	0.04	5.651	0.025	144.76	2.02	0.1458	0.0069	15628	87	14839	753	151.0	2.1
UAL14	ALV-3891-1646-004-004	4.921	0.004	12.04	0.05	1.496	0.015	144.77	1.08	0.1480	0.0017	15242	75	15071	182	151.1	1.1
UAB16b	ALV-3891-1725-005-007	7.041	0.004	48.79	0.21	3.167	0.014	119.86	0.37	0.4211	0.0034	51362	287	51014	522	138.5	0.5
UAB16	ALV-3891-1725-005-007	3.719	0.002	18.84	0.09	14.614	0.064	135.55	1.05	0.2902	0.0181	34517	208	32034	2328	148.4	1.5
UAB17	ALV-3891-1725-005-007	3.728	0.002	18.31	0.09	2.848	0.013	136.45	1.06	0.2963	0.0040	33269	197	32783	510	149.7	1.2
UAB18	ALV-3891-1725-005-007	4.039	0.003	19.81	0.10	1.817	0.008	139.59	1.05	0.2974	0.0026	33093	195	32805	337	153.2	1.2
UAB20	ALV-3891-1725-005-007	3.852	0.002	18.88	0.09	2.430	0.011	135.17	1.04	0.2963	0.0034	33232	194	32829	435	148.3	0.2
UAL10	ALV-3891-1725-005-007	3.734	0.002	18.38	0.08	3.722	0.018	143.52	1.06	0.2957	0.0052	33108	172	32455	657	157.3	1.2
UAI09	ALV-3891-1758-006-003	3.665	0.003	6.92	0.03	0.797	0.008	140.72	1.10	0.1142	0.0012	11619	63	11499	132	145.4	1.1
UAJ05	ALV-3891-1758-006-006	3.676	0.003	7.03	0.03	5.232	0.023	140.50	1.27	0.1095	0.0068	11771	59	11002	721	144.9	1.3
UAI07	ALV-3891-1758-006-007	4.058	0.003	9.43	0.04	0.782	0.007	143.38	1.10	0.1410	0.0012	14438	72	14329	128	149.3	1.1
UAB08	ALV-3892-1315-001-002	3.143	0.001	16.86	0.07	0.405	0.002	134.91	4.04	0.3271	0.0016	36951	256	36860	263	149.7	4.5
UAE09	ALV-3892-1315-001-003	3.829	0.002	10.08	0.04	2.548	0.011	143.54	1.16	0.1575	0.0034	16509	79	16133	374	150.2	1.2
UAO16	ALV-3892-1315-001-003	4.032	0.002	10.28	0.05	0.704	0.014	148.72	1.10	0.1549	0.0011	15865	82	15769	122	155.5	1.1
UAB11	ALV-3892-1315-001-007	6.668	0.004	27.07	0.12	8.491	0.036	137.16	1.17	0.2418	0.0062	26736	139	25977	746	147.6	1.3
UAB12	ALV-3892-1315-001-007	6.683	0.005	26.86	0.12	9.705	0.043	129.42	4.01	0.2385	0.0070	26651	177	25781	856	139.2	4.3
UAB13	ALV-3892-1315-001-007	6.520	0.003	26.34	0.11	8.511	0.036	136.04	1.03	0.2405	0.0063	26625	137	25848	755	146.4	1.1
UAB14	ALV-3892-1315-001-007	6.607	0.003	26.46	0.13	8.492	0.037	134.15	1.00	0.2384	0.0062	26410	150	25644	755	144.2	1.2
UAB15	ALV-3892-1315-001-007	6.409	0.003	25.92	0.12	8.325	0.036	134.50	1.06	0.2407	0.0063	26690	146	25915	763	144.7	1.2
UAL17	ALV-3892-1315-001-007	6.695	0.003	26.82	0.12	10.268	0.044	134.96	1.03	0.2369	0.0076	26393	132	25444	922	145.0	1.2
UAO15	ALV-3892-1315-001-007	4.540	0.002	17.65	0.08	3.239	0.019	135.98	1.08	0.2340	0.0036	25494	132	25071	431	146.0	1.2
UAB03	ALV-3892-1315-001-008	3.516	0.002	9.05	0.04	1.396	0.006	142.06	4.03	0.1552	0.0020	16123	101	15906	232	148.6	4.2
UAL16	ALV-3892-1315-001-008	3.525	0.002	9.15	0.04	0.756	0.007	142.43	1.08	0.1575	0.0013	16268	78	16145	142	149.1	1.1
UAB01	ALV-3892-1315-001-010	4.712	0.002	21.83	0.09	0.535	0.002	128.09	4.04	0.2825	0.0013	31372	211	31296	218	139.9	4.4

Lab ID	Database ID	^{238}U (ppm)		^{230}Th (ppt)		^{232}Th (ppb)		$\delta^{234}U_{initial,\ raw}$ (‰)		$(^{232}Th/^{238}U)_{act}$		Age_{raw} (yrs)		Age_{corr} (yrs)		$\delta^{234}U_{initial,\ corr}$ (‰)	
UAJ09	ALV-3892-1315-001-B4-SS3	3.622	0.003	9.41	0.04	0.685	0.008	142.81	1.16	0.1578	0.0012	16282	83	16173	134	149.5	1.2
UAE02	ALV-3892-1421-002-001-20	3.214	0.003	24.30	0.11	0.705	0.003	130.29	5.01	0.4608	0.0024	56719	482	56529	509	152.9	5.9
UAE01a	ALV-3892-1421-002-001-5	4.263	0.003	26.61	0.11	1.502	0.007	130.40	5.01	0.3795	0.0024	44549	350	44284	430	147.8	5.7
UAB07b	ALV-3892-1711-006-002	5.620	0.006	43.83	0.19	7.836	0.034	128.99	0.42	0.4696	0.0073	59154	355	58037	1192	152.0	0.7
UAB07	ALV-3892-1711-006-002	3.181	0.003	24.49	0.11	2.157	0.009	136.75	4.07	0.4670	0.0039	57607	457	57068	685	160.7	4.8
UAB02	ALV-3892-1711-006-004	3.687	0.003	21.08	0.09	0.929	0.004	134.34	4.04	0.3480	0.0020	39880	283	39704	323	150.3	4.5
UAB04	ALV-3892-1711-006-006	3.331	0.003	25.63	0.11	1.544	0.007	134.99	4.03	0.4678	0.0031	57686	453	57313	569	158.7	4.8
UAB10	ALV-3892-1711-006-008	3.384	0.002	19.37	0.09	0.808	0.003	140.16	4.05	0.3484	0.0020	39669	283	39503	318	156.7	4.5
UAB06	ALV-3892-1711-006-010	3.250	0.003	18.64	0.08	0.943	0.004	133.01	4.05	0.3490	0.0021	40099	287	39896	340	148.9	4.5

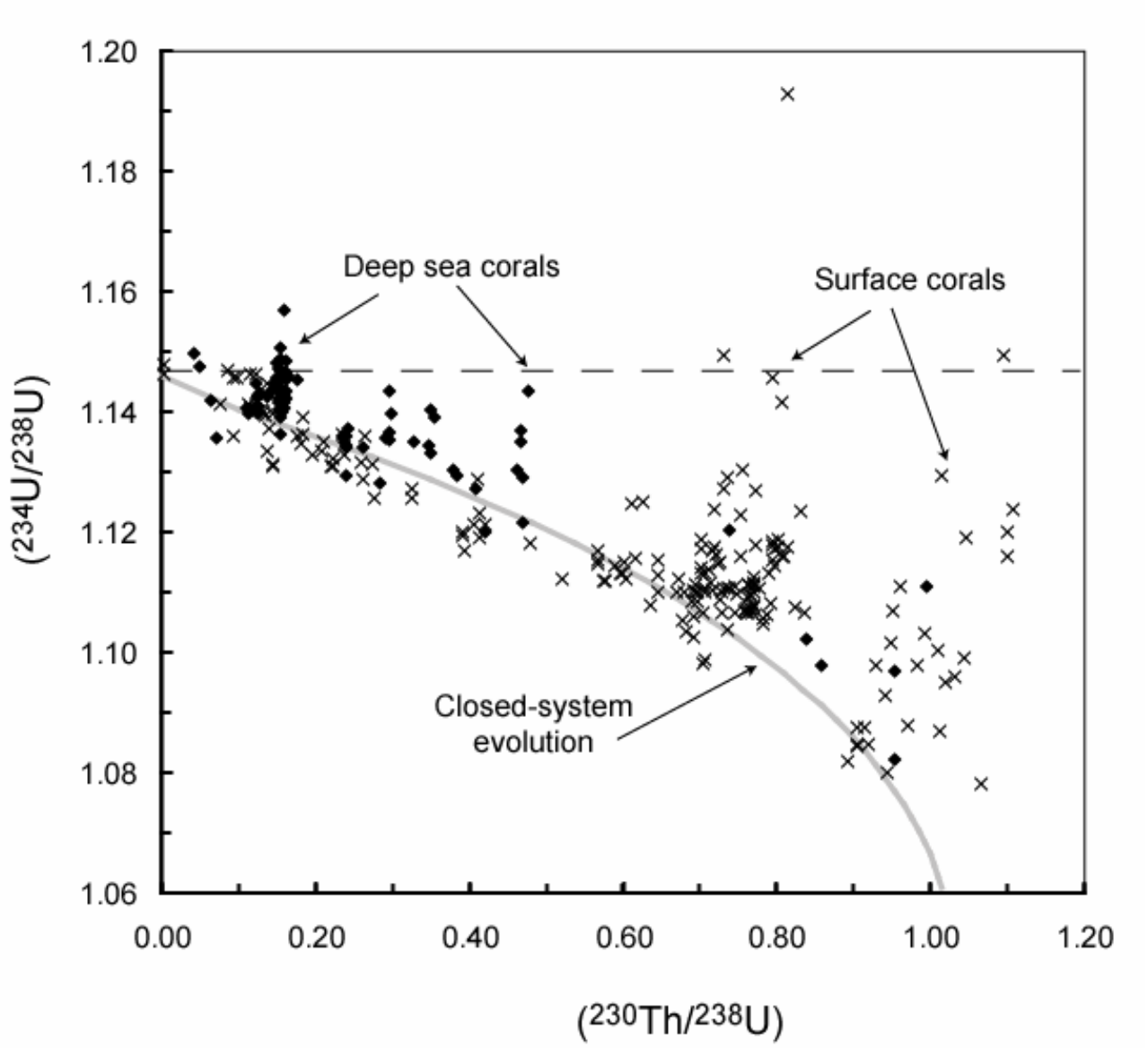
1.20
1.18
1.16
1.14
1.12
1.10
1.08
1.06
0.00
0.20
0.40
0.60
0.80
1.00
1.20
(234U/238U)
(230Th/238U)
Deep sea corals
Surface corals
Closed-system
evolution

Figure 1

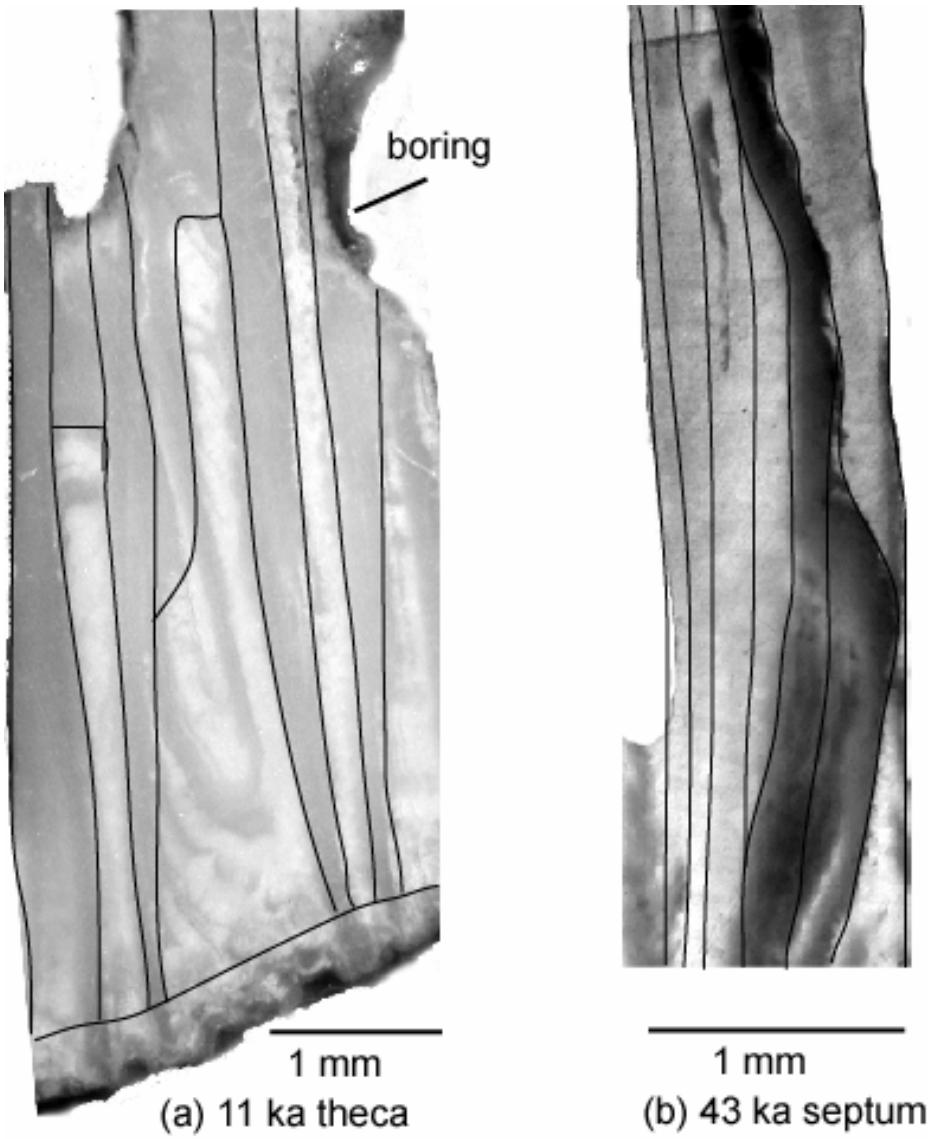

Figure 2

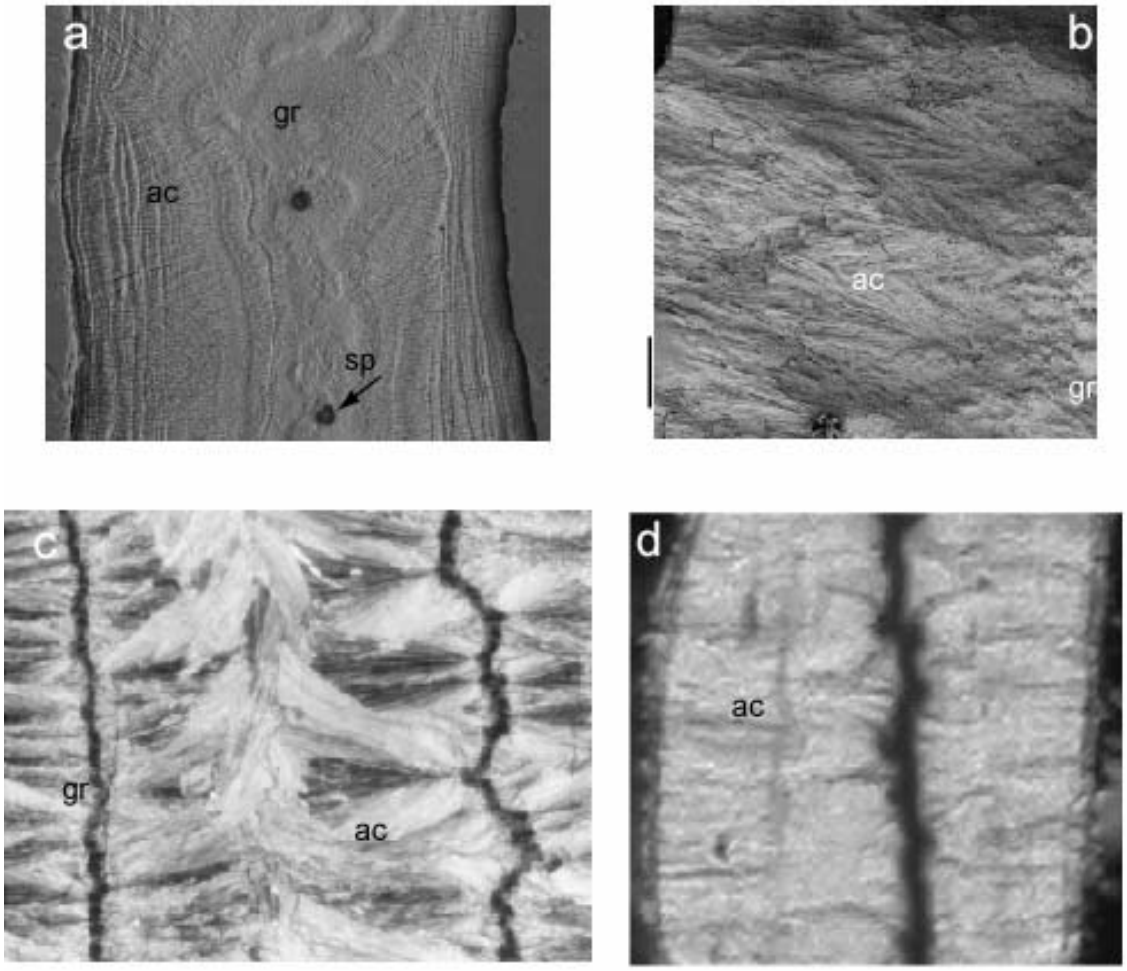

Figure 3

A

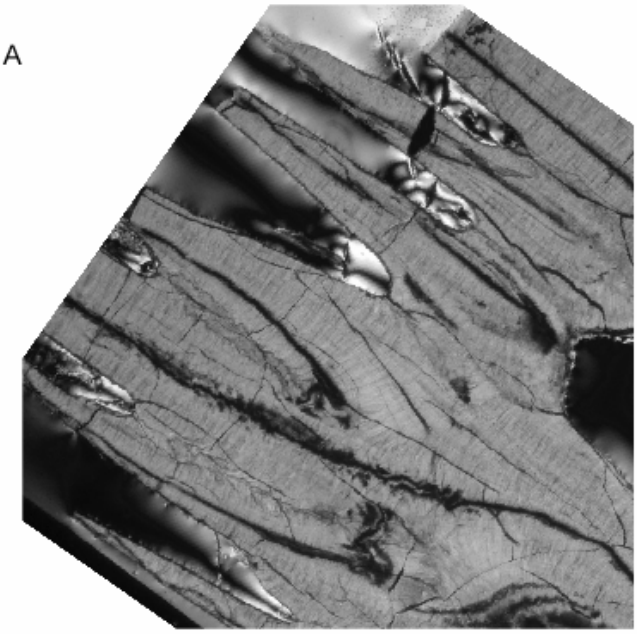

B

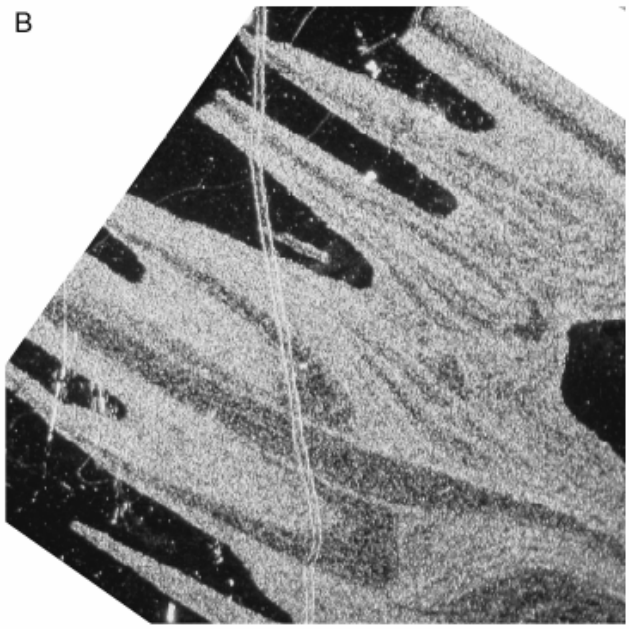

Figure 4

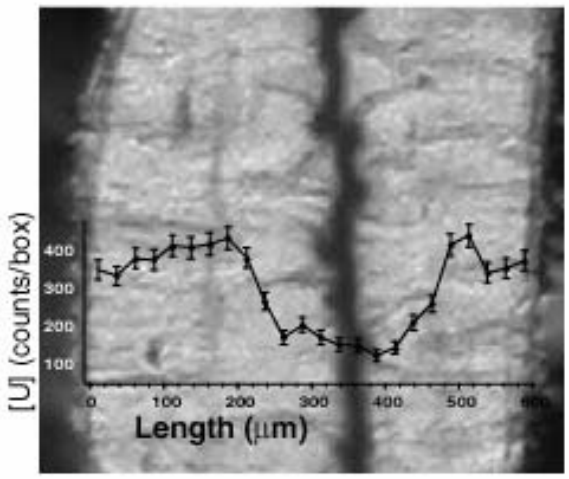

Figure 5

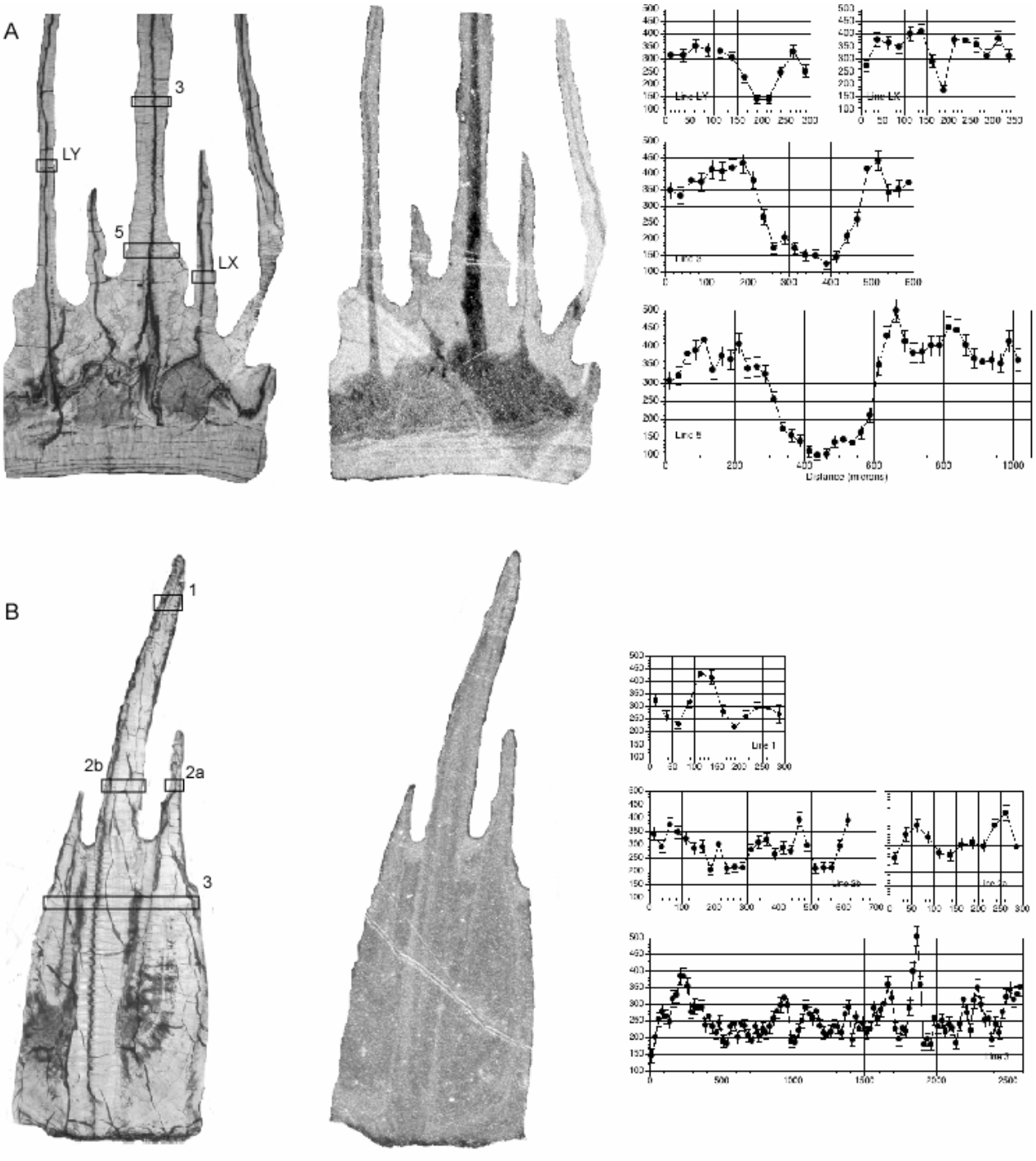
A
3
LY
5
LX
B
1
2b
2a
3
Line LY
Line LX
Line 5
Distance (microns)
Line 1
Line 3

Figure 6

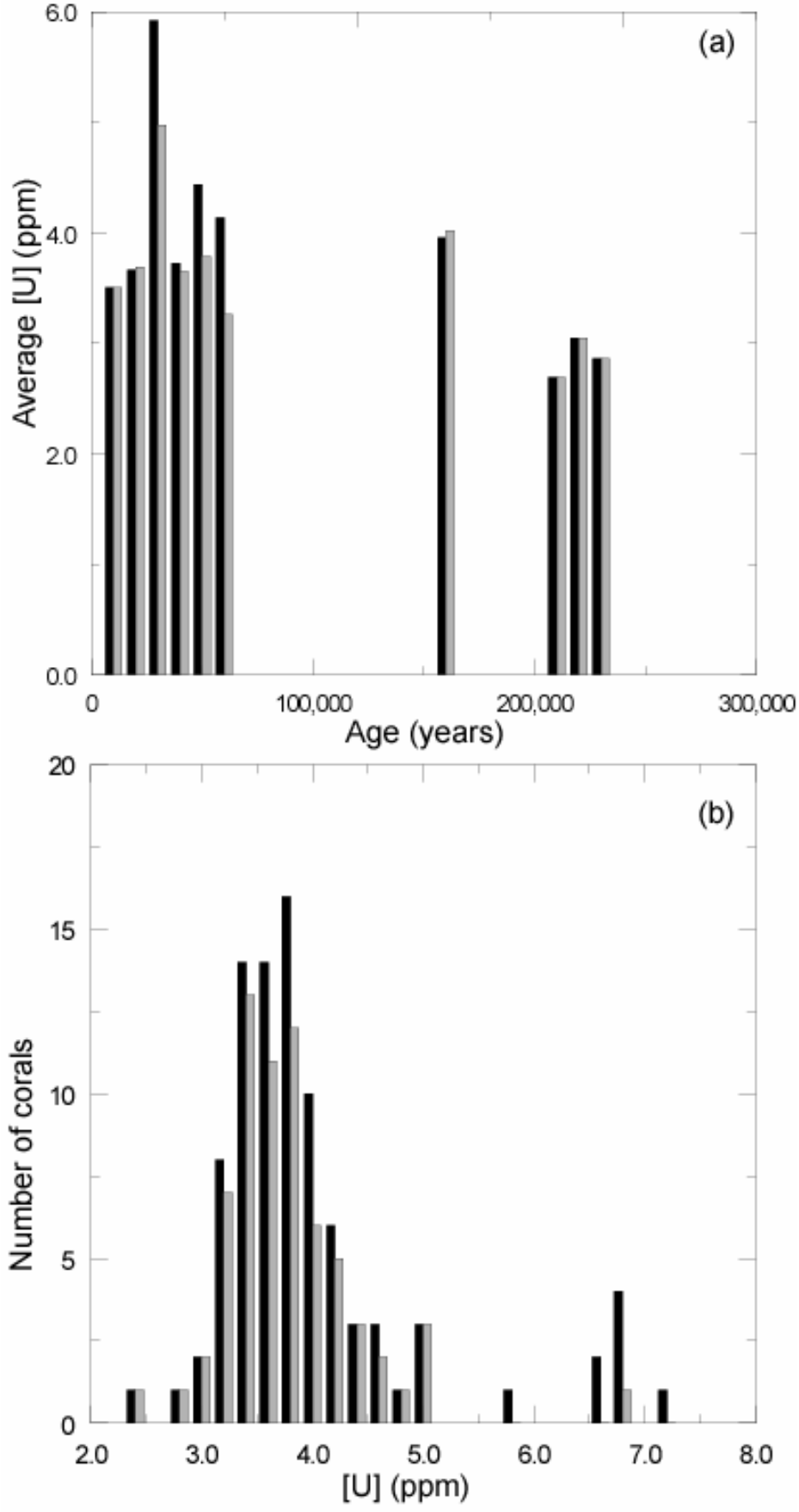
(a)
Average [U] (ppm)
6.0
4.0
2.0
0.0
0
100,000
200,000
300,000
Age (years)
(b)
Number of corals
20
15
10
5
0
2.0
3.0
4.0
5.0
6.0
7.0
8.0
[U] (ppm)

Figure 7

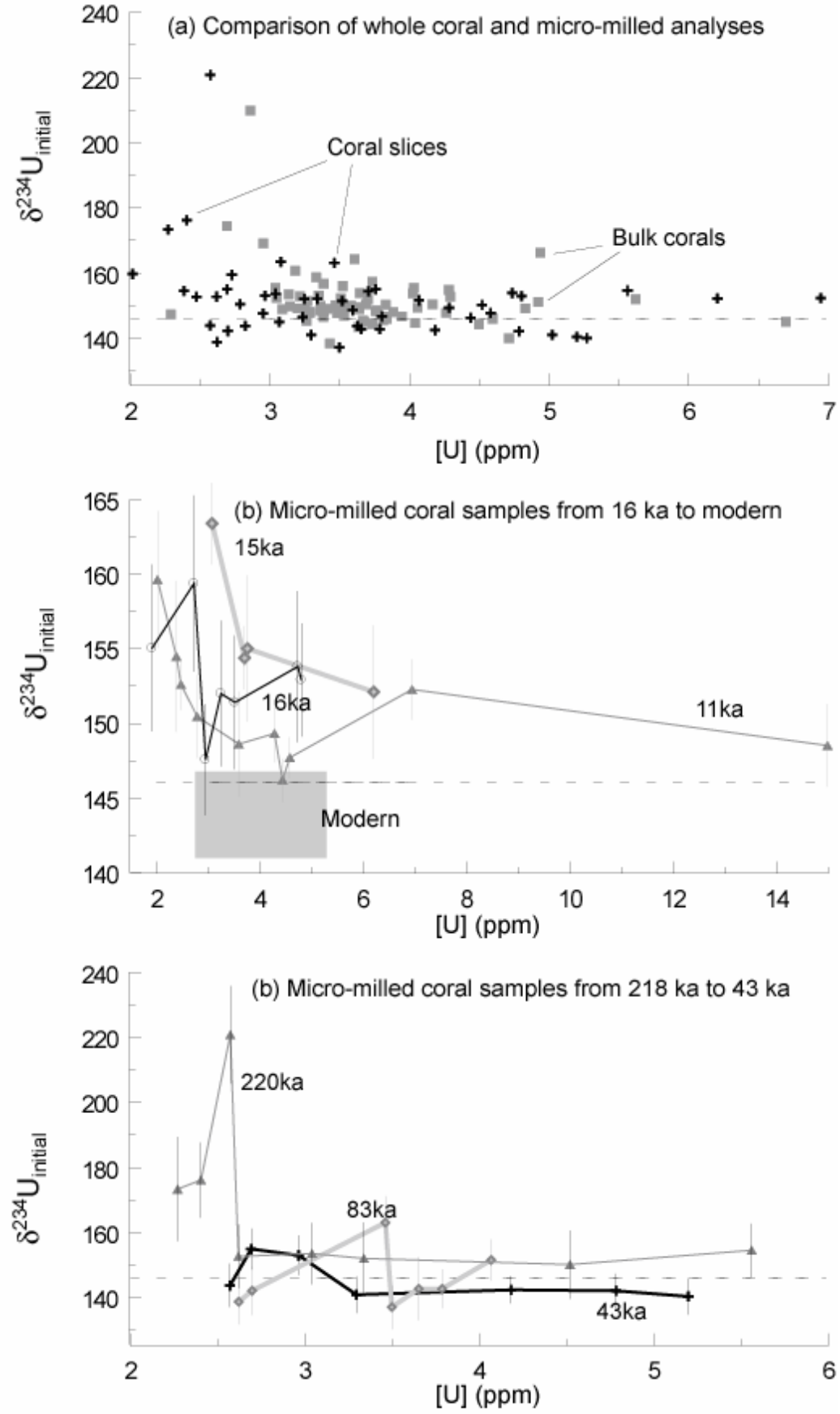
(a) Comparison of whole coral and micro-milled analyses
Coral slices
Bulk corals
δ234Uinitial
[U] (ppm)
(b) Micro-milled coral samples from 16 ka to modern
15ka
16ka
11ka
Modern
δ234Uinitial
[U] (ppm)
(b) Micro-milled coral samples from 218 ka to 43 ka
220ka
83ka
43ka
δ234Uinitial
[U] (ppm)

Figure 8

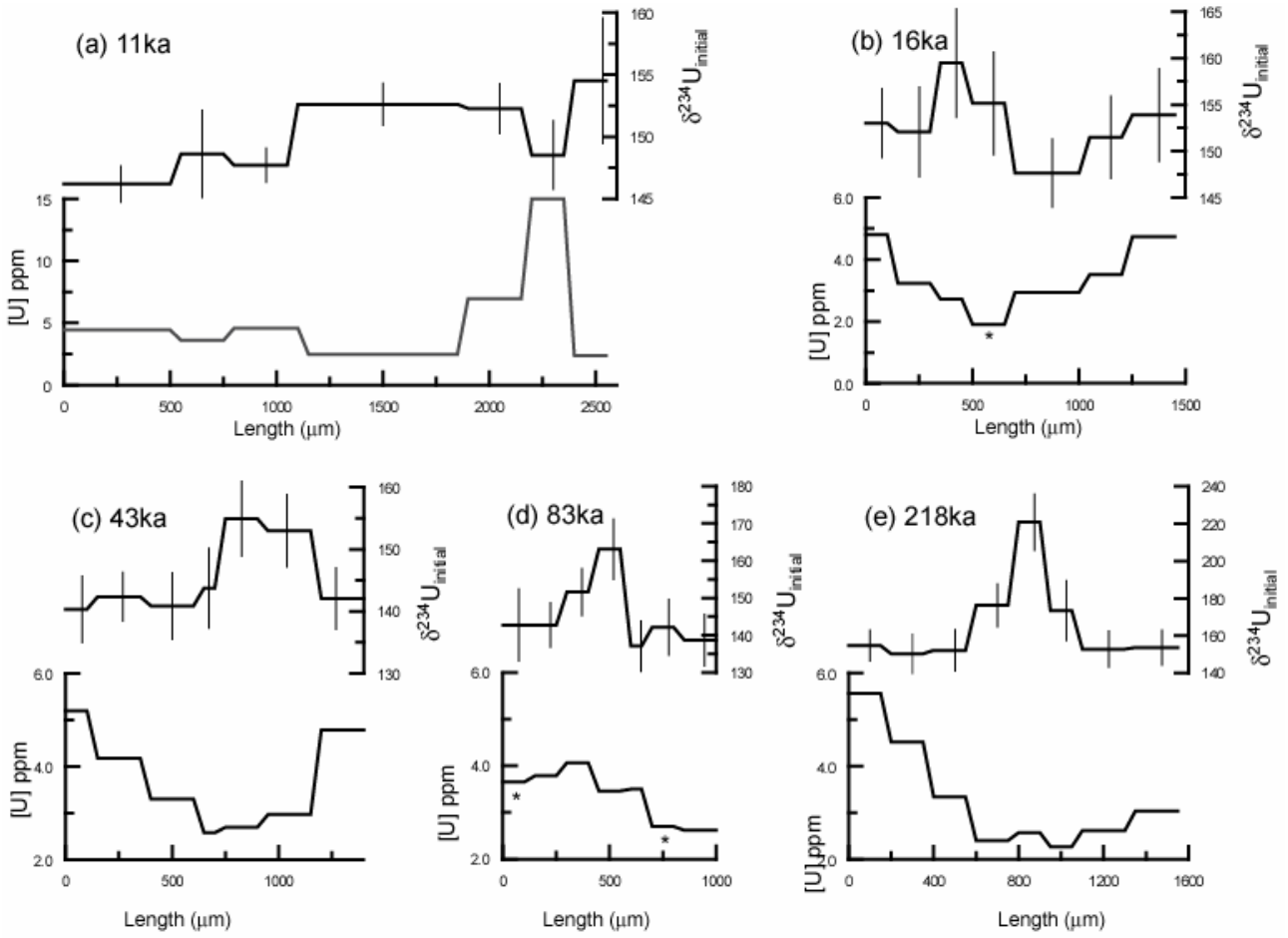
(a) 11ka
(b) 16ka
(c) 43ka
(d) 83ka
(e) 218ka
[U] ppm
Length (μm)
δ234Uinitial

Figure 9

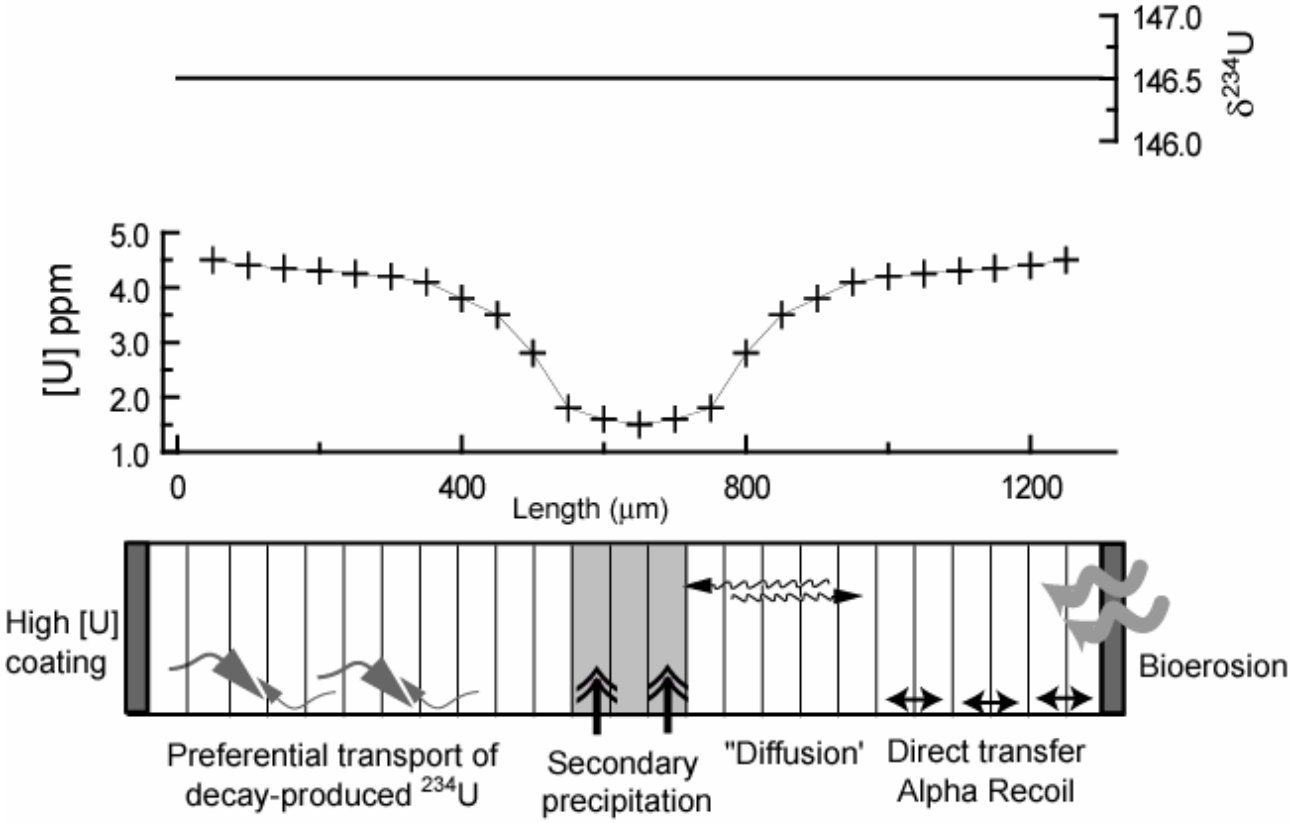
147.0
146.5
146.0
δ234U
[U] ppm
5.0
4.0
3.0
2.0
1.0
0
400
800
1200
Length (μm)
High [U]
coating
Bioerosion
Preferential transport of
decay-produced 234U
Secondary
precipitation
"Diffusion'
Direct transfer
Alpha Recoil

Figure 10

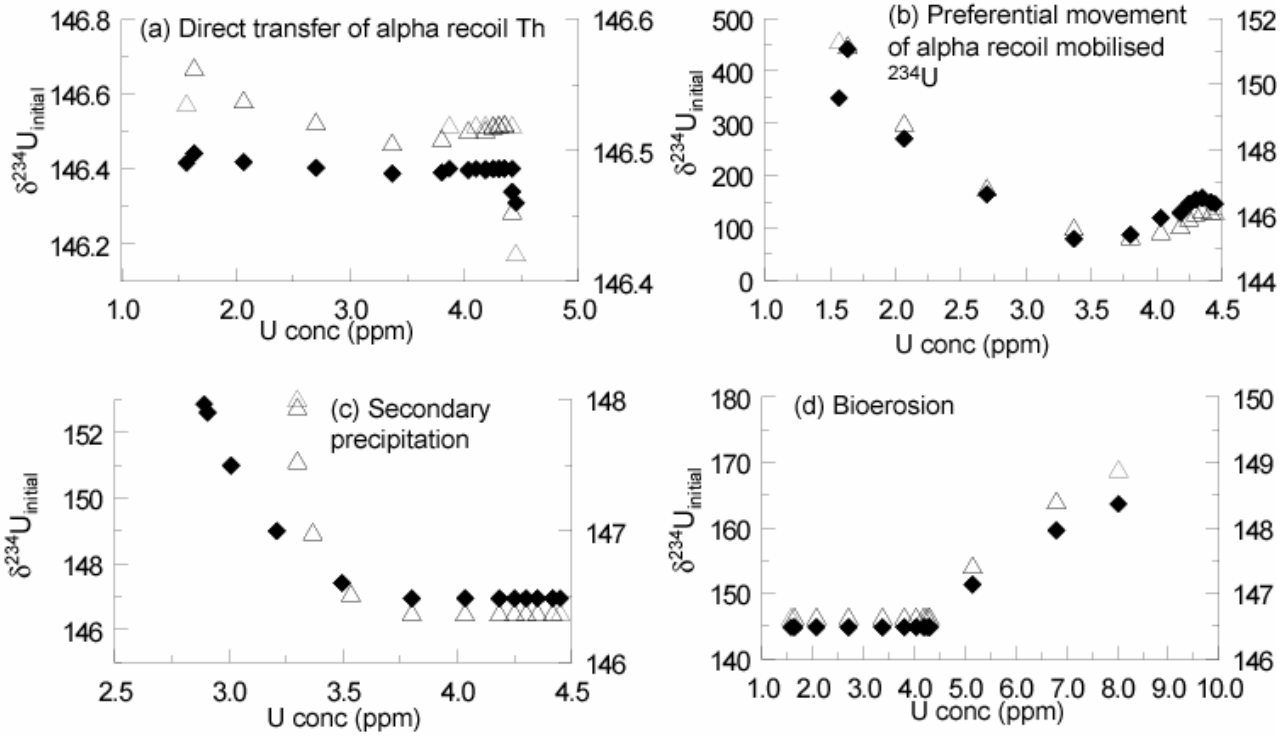
(a) Direct transfer of alpha recoil Th
(b) Preferential movement of alpha recoil mobilised ^{234}U
(c) Secondary precipitation
(d) Bioerosion
$\delta^{234}U_{initial}$
U conc (ppm)

Figure 11

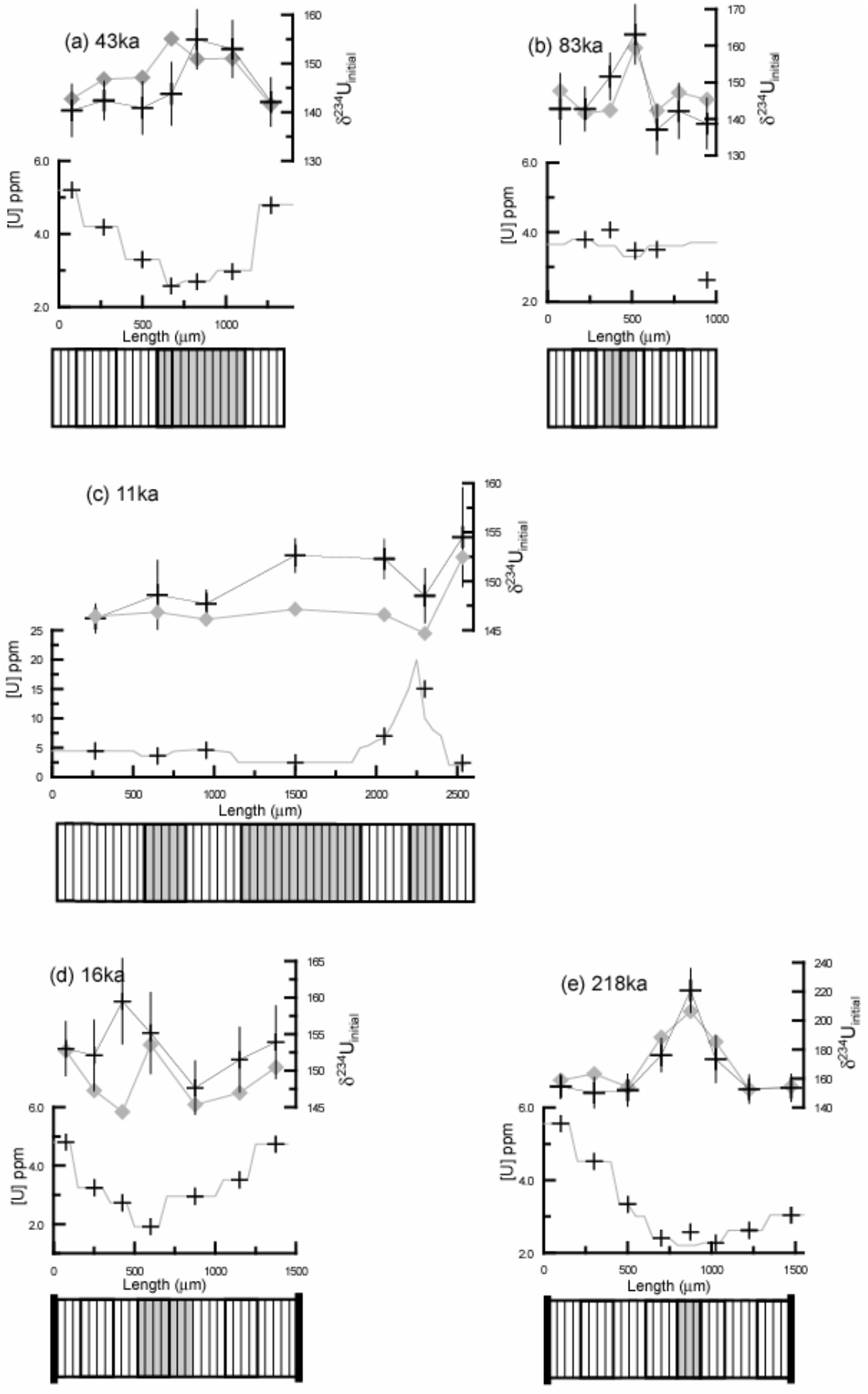
(a) 43ka
(b) 83ka
(c) 11ka
(d) 16ka
(e) 218ka
[U] ppm
Length (μm)
δ234Uinitial

Figure 12